



Weidong Xiang and Jiasong Zhong

Contents

Introduction	622
Sol-Gel Preparation Process of Borosilicate Glasses	623
Analysis of the Sol-Gel Process of Na ₂ O–B ₂ O ₃ –SiO ₂ (NBS) System	624
Analysis of Influence Factors	626
Sol-Gel Transition Process from Gel to Glass	631
The Sintering and Preparation Process of System Glass	631
The Composition of NBS System Xerogel and Glass	632
The Property of the NBS System Glass	632
The Structural Analysis of the Formation Process from Gel to Glass	633
The Common Hybrid Borosilicate Glass	639
Metal and Metal Oxide Nanoparticles Doped Borosilicate Glass	639
Nanoalloy Quantum Dots Doped Glass	645
Sulfide Quantum Dots Doped Glass	648
Formation Mechanism of Nanocrystals in Borosilicate Glass	652
Organic Compounds Quantum Dots Doped Glass	653
Concluding Remarks	661
References	661

Abstract

Borosilicate glass has excellent chemical durability and remarkably low thermal expansion coefficient, which draws great attention to laboratory equipment and optical devices. In this chapter, the preparation process of borosilicate glass and

W. Xiang (✉)

College of Chemistry and Materials Engineering, Wenzhou University, Wenzhou, China
e-mail: xiangweidong001@126.com

J. Zhong (✉)

College of Materials and Environmental Engineering, Hangzhou Dianzi University, Hangzhou, China
e-mail: jjiasongzhong@hdu.edu.cn

transition process from gel to glass by sol-gel method are summarized in detail, especially, the factors for the preparation of transparent glass. Impressively, compared to pure glass material, transparent glass doped metal or semiconductor nanoparticles exhibit unique and excellent optical properties. Additionally, a series of quantum dots concluding sulfur, metal and oxides, and organic compounds quantum dots doped sodium borosilicate glasses are displayed. Finally, the relationship between microstructure and optical property is analyzed in depth.

Introduction

As it is well known, borosilicate glass has excellent chemical durability compared to ordinary glass. The remarkably low thermal expansion coefficient ($\sim 3.3 \times 10^{-6}/^{\circ}\text{C}$ at room temperature) endows borosilicate glass eminent resistance to thermal shock and breaking (Park and Lee 1995; Boccaccini et al. 2007). Such superior properties make borosilicate glass widely used in laboratory equipments and optical devices. Among them, sodium borosilicate glass is a typical spinodal phase separation glass and source material for porous glass, which has widespread application in many industries (Angeli et al. 2012). Aside from the many industrial and consumer-oriented applications, these glasses are leading candidates for encapsulation of reprocessed commercial and defense-related nuclear waste (Hervig and Navrotsky 1985). As a result, much effort has been input to develop these glasses. M. E. Milberger (Milberger et al. 1972), Y.H. Yun (Y.H. Yun et al. 1978), H. Doweidar (Doweidar et al. 1988), and A. Grandjean (Grandjean et al. 2008) have studied the sodium silicate glass by nuclear magnetic resonance, analyzing the percentage of B atoms in $[\text{BO}_4]$ tetrahedral with the composition of glass. K. Sun (Sun et al. 2004) has studied the phase structure of sodium borosilicate glass as well as the pore structure of sodium borosilicate glass. G. Bureau (Bureau et al. 2008) has carried on the molecular dynamics on the structure by the energy deposition methods. M.H. Bartl (Bartl et al. 2001), R. K. Mishra (Mishra et al. 2007), M. S. Gaafar (Gaafar and Marzouk 2007), and J. Matsuoka (Matsuoka et al. 2008) have synthesized sodium borosilicate glass doped with different oxides to discuss the influence of optical and electrical properties of glass. However, all of the discussed above are prepared by melting method in high temperature, which is a traditional method to fabricated glass vessels and function glass. Recently, scientific workers explore a novel method to prepare sodium borosilicate glass by sol-gel method combining atmosphere control. By sol-gel method, the as-prepared sodium borosilicate glass has several advantages, such as good uniformity of composition, and uniform doping oxide, metal, and sulfide nanocrystals. Therefore, a series of semiconductor and metal nanoclusters doped sodium borosilicate glass have been reported by sol-gel method, such as P. Rumori reported the sodium borosilicate glass doped Mn^{2+} , and studied the electron spin resonance effect produced by Mn^{2+} (Rumori et al. 1998). Importantly, our team is engaged in sodium borosilicate glass, and a series of sulfur, metal, and oxide quantum dots have been successfully doped in sodium borosilicate

glass, and the relationship between microstructure and nonlinear optical nonlinearity have been studied in depth (Xiang et al. 2012, 2013; Zhong et al. 2012a, b, 2013a, b, c, 2014a, b; Pei et al. 2014; Yang et al. 2011a, b, c, d). Thus, in the chapter, we introduced in detail the sol-gel process of sodium borosilicate glass and factors for the preparation of transparent glass.

Sol-Gel Preparation Process of Borosilicate Glasses

The sol-gel method, which allows the preparation of glassy materials at low temperature, has attracted increasing interest with many advantages, particularly for certain glass compositions which are difficult to prepare by conventional melting. Sol-gel is a chemical synthesis technique for preparing materials such as thin films, glass, ceramics, and powders. Especially, the sol-gel method is interesting for synthesizing glass because of the homogeneous distribution of the components, and the possibility of porosity and particle size control (Cartaa et al. 2007). In the sol-gel method, a system of colloidal particles in a solution (sol) becomes a network (gel), by the linking of particles together in a basic reaction process consisting of hydrolysis and condensation reactions (Brinker and Scherer 1990; Klein 1994; Heshmatpuor et al. 2011; Sakka 2005). And sol-gel process needs either controlled drying that is slow or supercritical drying process to obtain porous materials in the form of alcogel, xerogel, or aerogels. Dried gels have a large number of pores in their body so that it is a potential method to prepare porous materials with a variety of pore size distributions or pore volumes by controlling gelation reactions and the drying–heating schedule (Osaka et al. 1988). Such pores can be used as hosts to accommodate nanoparticles of metal complexes or metal ions (Song et al. 2003).

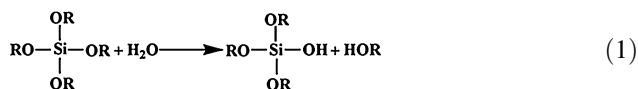
Preparation of sodium borosilicate xerogel system is a very meaningful research, because it not only has similar characteristics of SiO_2 glass prepared by sol-gel method but also has lower sintering temperature compared to SiO_2 glass. Meanwhile, sodium borosilicate glass prepared by sol-gel and heat treatment method undergoes the phase change of solution–xerogel–glass, during which chemicals can be easily doped and well dispersed, porous structure can be naturally formed, and substances doped can be well encapsulated and preserved. Therefore, borosilicate glass is a competitive base glass to load quantum dots or nanoparticles. Sol-gel technology can not only be applied to prepare powders, fibers, and film materials but also to prepare monolithic glass materials. The sol-gel process produces porous, disorder, dendritic, and consecutively network-structured colloid particles in the solution, and the obtained wet gel can mainly form two categories of porous materials: aerogel and xerogel (stiff gel) through different processing conditions. These early investigators observed that the hydrolysis of tetraethyl orthosilicate (TEOS), $\text{Si}(\text{OC}_2\text{H}_5)_4$, under acidic conditions yielded SiO_2 in the form of a glass-like material. Many factors such as the composition of chemical precursor and solvent, catalyst, and the dehydration and condensation reaction temperature, even the container employed, have important influence on the preparation of excellent stiff gel.

Analysis of the Sol-Gel Process of Na₂O–B₂O₃–SiO₂ (NBS) System

The process of preparing NBS glass by sol-gel method mainly includes (a) the stoichiometric ratio of sodium, boron, and silicon precursors dispersed in the solvent; (b) after hydrolysis reaction, formed active monomers, through polymerization, begin to be sol and then generate gel with a certain space structure; (c) after drying and heat treatment, the NBS glass forms. The overall reaction can be divided into the following.

Hydrolysis

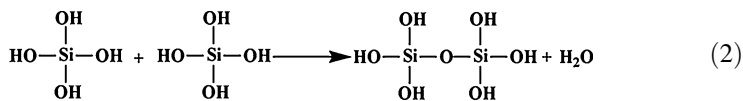
Nonionizing type molecular, metal alkoxide M(OR)_n (n is the valence state of metal M, M = Si, R is for alkyl) reacts with water and generates M(OH)_n. Especially, using the acid as catalyst, the hydrolysis reaction is mainly the electrophilic substitution where OR is removed by H⁺. The chemical equation is as follows:



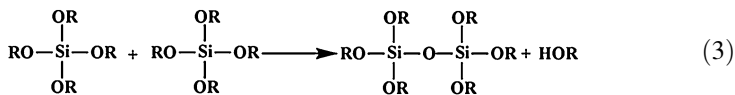
Polymerization Reaction

In the transition process of the sol-gel, the TEOS mainly exists in the form of Si–(O–Si)₄ (Q₄), Si–(O–Si)₃(OH) (Q₃), and Si–(O–Si)₂(OH)₂ (Q₂). According to the sort of take off, molecules in the reaction process can be divided into:

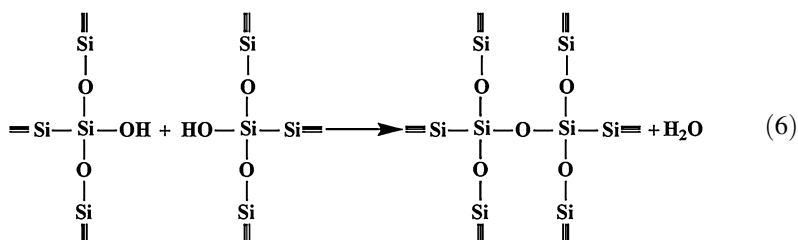
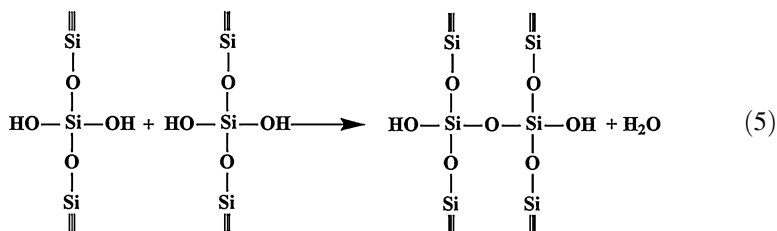
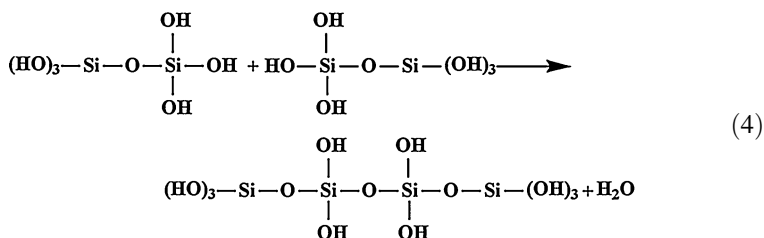
(a) Water condensation



(b) Alcohol condensation



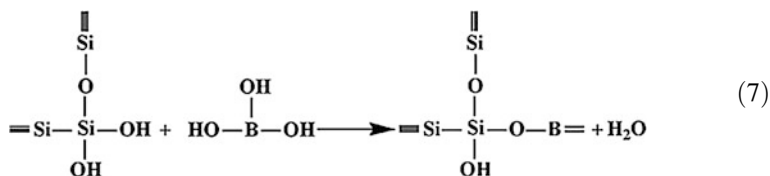
In the initial stage of room temperature, generally speaking, polycondensation reaction is two polymerizations, which lead to the silanol content decreasing. These results are not conducive to the continued growth of molecular chain and the increase of molecular weight. With the increase of temperature, the product will further polycondense, making the chain molecules to a dendritic structure; the chemical reaction can be shown as follows:

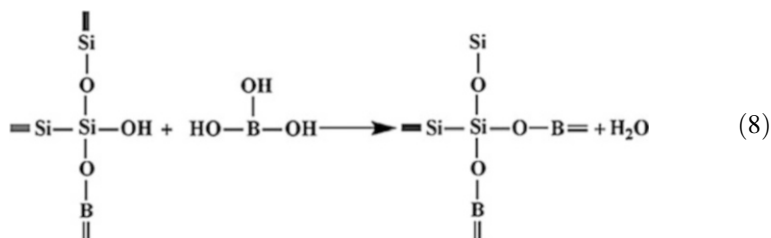


Based on the above equation, we can find that a silicon connecting with two bridge oxygen, three bridge oxygen, and four bridge oxygen groups exist, which occurs at the same time under low temperature. With the temperature increasing, the gel transform into glass, and the reaction mainly taking place in equation (6), that is to say, a dense network of silicon oxygen tetrahedron structure, is formed.

The Introduction of Boric Precursor

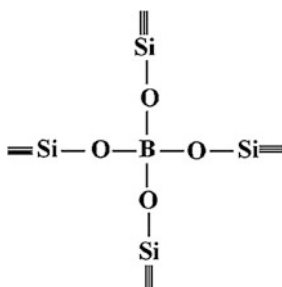
Boric acid (H_3BO_3) as B_2O_3 body former involved in the reaction system. The boric acid will participate in the dehydration reaction at a high temperature, which intakes B into the silica network system to form Si-O-B bond, as follows:





The Transition Process

Na_2O can provide free oxygen at a high temperature; boron can be easily added to the silica network in the form of four-coordinate mode. On the other hand, the addition of sodium ethoxide also increased the polymerization degree of silicon.



However, the actual reaction process to form a transparent and block dry gel is very complicated; a large number of affecting factors exist in the process. The structure and reaction rate of the product depends on the catalyst, solvent, concentration of reactant, drying and heat treatment process, and other factors.

Analysis of Influence Factors

Effects of Precursors and Solvents on the Properties of Gels

In order to prepare a transparent multicomponent sodium borosilicate stiff gel, except the consideration of hydrolysis and condensation, we must firstly consider the mutual solubility of a precursor in the solution according to the law of solubility, because the preparation of a stiff gel is a very complicated process which involves physical change and chemical reaction. Based on the principle of the dissolution in the similar material structure, the solvent whose structures or the part structures are similar to precursor could be selected as each precursor solvent. Solubility is very important for the preparation the monolithic gel.

In the experiment, SiO_2 is introduced by tetraethyl orthosilicate (TEOS) dissolved methanol or ethanol, while B_2O_3 is incorporated in the form of boric acid, and

methanol, ethanol, and ethylene glycol dimethyl ether are used as the appropriate solvent. In addition, sodium methoxide in methanol solution, sodium ethoxide ethanol solution, or aqueous sodium acetate are selected to introduce Na_2O . On this basis, we are focusing on the effects of precursors of sodium and the precursor solvent of TEOS and boric acid on gel properties. The results are detailed in Table 1.

Due to the H_2O molecule containing OH group, which is same to methanol, ethanol, and ethylene glycol monomethyl ether, so water is miscible with the solvents when Na_2O is introduced in the form of NaOAc solution; as a result corresponding sol is uniform and transparent. However, compared to water, the solubility of NaOAc in ethanol, methanol, and ethylene glycol methyl ether is smaller. Thus, when the wet gel turns to dry gel, the saturated NaOAc solution will separate out through precipitation due to the evaporation of the solvent.

The solubility of boric acid in ethanol is very small (5.6 g H_3BO_3 /100 mL HOET at 20 °C). Therefore, if we take ethanol as solvent of boric acid, we will waste much ethanol and introduce little boric acid, even though a stiff gel can be successfully prepared. Besides, excessive solvent will increase the amount of volatile undoubtedly and extend the gel aging, drying time, which was easy to crack during the drying process.

Based on the above analysis, we can conclude that the optimal solvents are TEOS and sodium dissolved in ethanol, while boric acid is soluble in ethylene glycol monomethyl ether.

Effects of Dry Temperature on Gel Time (t-Gel)

In NBS system, the gel time is the time flowing sol turns to steady gel, which is greatly influenced by the temperature. Figure 1 shows the relationship between gel time and temperature, indicating that the gel time decreases rapidly with the increase of the temperature mainly attributed to the release of water molecules, alcohols, and other organic solvents. However, the gel time decreases gradually as the temperature increases higher than 50 °C.

Influence of Contents of the Catalyst on the Properties of Gel

In the process of sol-gel experiments, we often drop concentrated hydrochloric acid as a catalyst, which can restrain the reaction rate of alkoxide in the process of hydrolysis and polycondensation. As shown in Table 2, with the increase of hydrochloric acid catalyst, gel time slightly decreased, and color changed from colorless transparent gel to light blue. The electrophilic attack will occur due to the addition of acid catalyst leading to H_3O^+ ions produced. Therefore, the hydrolysis reaction can be analyzed by the electrophilic mechanism. Early in the process, the positively charged ions more easily react with monomer ion containing OR group; thus, hydrolysis is very fast. And then, with increasing of molecular chain and diminishing the OR group, the hydrolysis rate gradually reduced. Meanwhile, the pH value of the sol is changed by adding concentrated hydrochloric acid, and hydrolysis and condensation rate are accelerated under high pH value. Under this condition, the

Table 1 Properties of sol and gel by using methanol as solvent of TEOS

State	Sodium-methanol		Sodium-ethanol		Sodium acetate-water	
	$H_3BO_3-CH_4O$	$H_3BO_3-C_3H_8O_2$	$H_3BO_3-CH_4O$	$H_3BO_3-C_3H_8O_2$	$H_3BO_3-CH_4O$	$H_3BO_3-C_3H_8O_2$
Sol	Clear	Clear	Turbid	Clear	Clear	Clear
Wet gel	Transparent bulk	Transparent bulk	Turbid	Transparent bulk	Transparent bulk	Transparent bulk
Dried gel	Transparent bulk	Transparent bulk	Turbid pulverized	Transparent bulk	Pulverized	Pulverized

Fig. 1 The relationship of dry temperature versus gel time

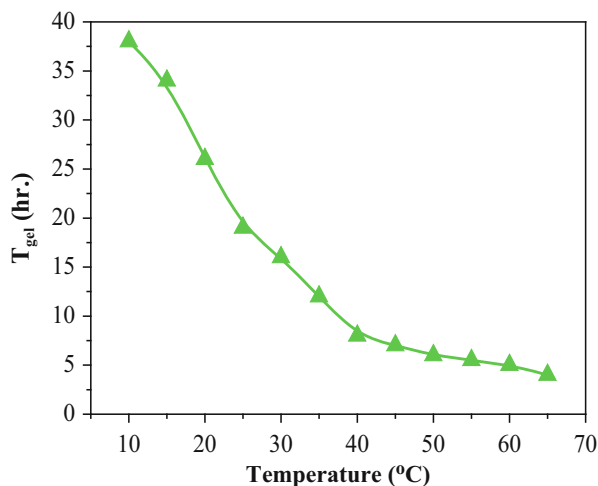


Table 2 Effects of catalyst on the properties of gel

H ₂ O:HCl:HOEt:Si(OEt) ₄ :H ₃ BO ₃ :NaOEt (molar ratio)	Sol	Gel	Stiff gel	T _{gel} /h
2:0.0054:2:1:0.69:0.18	Clear	Colorless	Colorless bulk	37
2:0.0071:2:1:0.69:0.18	Clear	Colorless	Colorless	36.46
2:0.0108:2:1:0.69:0.18	Clear	Light blue	Light blue bulk	36.35
2:0.0135:2:1:0.69:0.18	Clear	Light blue	Light blue bulk	36.26

as-formed particles dissolve aggravatingly, which leads to the delayed reunion and gelation process. Therefore, high porosity, big pore diameter, and high specific surface area would be formed under the environment of high pH. In contrast, densification and small specific surface area will be obtained under a very low pH (<2).

Shrinkage at Drying Treatment

In the process of dry treatment, wet gel has a great shrinkage due to the complex physical and chemical processes. Wet gel diameter shrinkage rate versus time in the drying process is shown in Fig. 2, in which HTHS dry curve is measured by high temperature thermal saturation method, while RTSR (Room Temperature Slow Release) dry curve is obtained by slowly release method at room temperature. The diameter shrinkage of wet gel diameter is 56% by HTHS (High Temperature Heat Saturation) method and 50% by RTSR (Room Temperature Slow Release) drying method, and the former method is easy to prepare transparent, cracking-free stiff gel.

Fig. 2 The relationship of shrinkage rate of diameter versus times

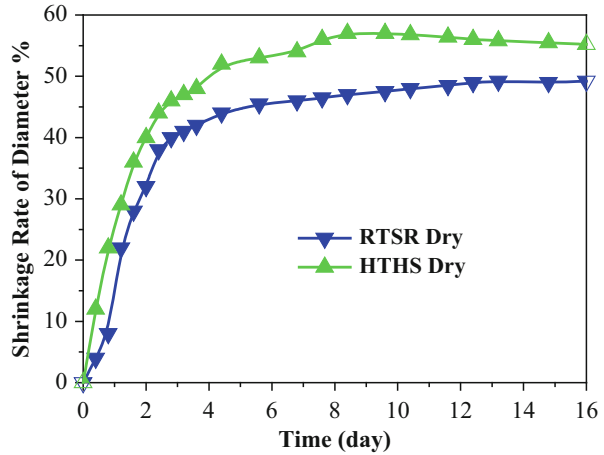
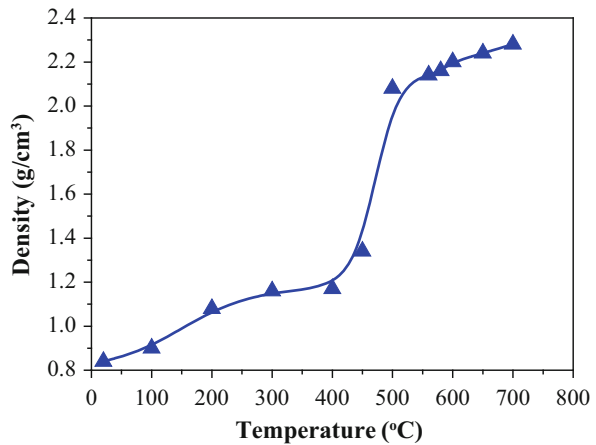


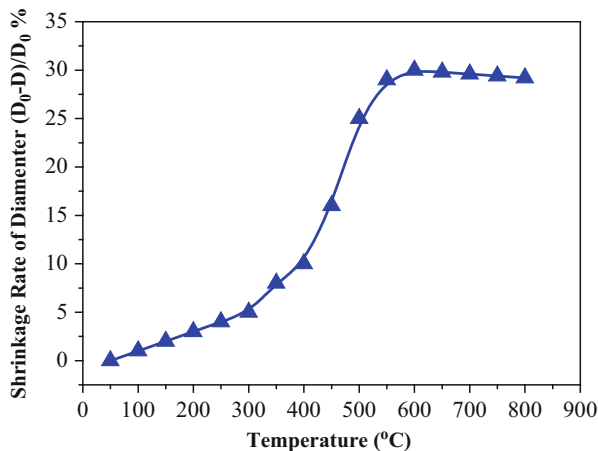
Fig. 3 Effects of sintering temperature on the density of gel



The Property of the NBS Dry Gel

Figures 3 and 4 show the effect of sintering temperature on the density and shrinkage rate of the diameter of NBS dry gel. From Fig. 3, we can see that the density of NBS dry gel increases as the temperature increases from 20 °C to 700 °C. When the sintering temperature is above 450 °C, the density of dry gel increases rapidly. However, as the sintering temperature rises higher than 550 °C, the glass density remains the same, and the maximum density reaches to 2.26 g/cm³. As seen from Fig. 4, the shrinkage rate of the diameter of NBS dry gel is enhanced as the temperature increases. When the sintering temperature reaches 450 °C, the shrinkage rate of the diameter increases largely. However, as the temperature increases to

Fig. 4 Effects of sintering temperature on shrinkage rate of the diameter of gel



550 °C, the value reaches the maximum (30%), and the shrinkage rate of the diameter is the same even if the temperature is increased.

Sol-Gel Transition Process from Gel to Glass

The preparation of aerogel usually comes from a supercritical drying process, which removes the rest of the solution in the wet gel without changing the gel state structure. Thus, low density, amorphous solid materials can be produced. On the other side, the xerogel is usually derived from an ordinary drying process that removes the residual solution and progressively changes the porous structure to a smaller one. As the structure changes reach a certain limit, the densification of porous xerogel can form bulk glass. The sol-gel approach can produce glass in the high-temperature phase separation zone, or below the crystallization temperature, which expands the scope of the glass formation. So far, reports on the preparation of NBS glass by sol-gel method have emerged, but few reports employ boric acid as the B_2O_3 precursor, and intensive researches on the formation mechanism of xerogel and glass have never been conducted. Herein, we employ boric acid as the B_2O_3 precursor and synthesized bulk NBS-based glass by sol-gel method and studied the basic law and technological process of the transformation from solution to gel, then to the formation of bulk glass.

The Sintering and Preparation Process of System Glass

In the process of sintering, several improper conditions will produce cracks and other defects, including:

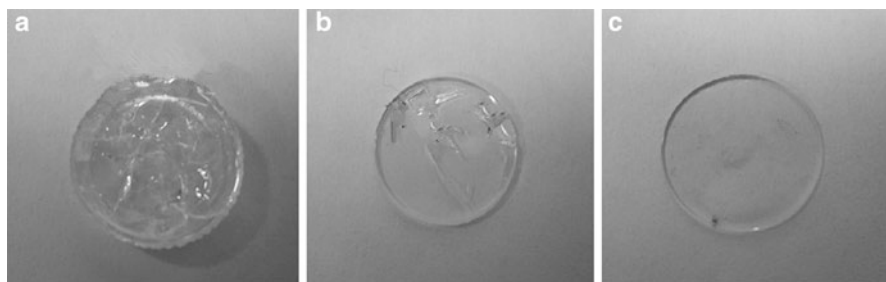


Fig. 5 The impact on glass integrity of different heating rates: (a) 10 °C/1 h, fragmentation; (b) 10 °C/2 h, cracking; (c) 10 °C/3 h, complete

1. Sintering of xerogel in the tube furnace in oxygen atmosphere, the fast heating rate and the fast oxygen flow impact and fracture the specimen easily. When the heating rate is below 4 °C h⁻¹, the preparation of colorless and transparent bulk glass with no cracks will be realized, as shown in Fig. 5.
2. Given no oxygen in the tube furnace, whatever sintering process is applied, the transparent bulk glass is impossible to form.
3. Glasses sintered in the muffle furnace usually colors in light brown or gray, but the slow heating rate and insulation sintering conditions will produce colorless and transparent bulk glass.

The Composition of NBS System Xerogel and Glass

Table 3 shows the chemical composition and the weight loss of the xerogel obtained by high-temperature heat saturation method, and the NBS system glass sintered for 12 h at 700 °C. The samples are sintered from room temperature to 900 °C and kept for 2 h at the heating rate of 180 °C h⁻¹. After being sintered from room temperature to 900 °C and kept for 2 h at the heating rate of 180 °C h⁻¹, the xerogel shows a weight loss of 21.20%, while the glass just shows a weight loss of 0.06%. The corresponding chemical composition of the xerogel composition is close to the theoretical composition, while the sintered glass has a lower B₂O₃ content and higher Na₂O and SiO₂ content, which mainly results from the volatile loss of B₂O₃ in the sintering process.

The Property of the NBS System Glass

Table 4 displays the density, microhardness, and refractive index of the glasses obtained by different heat treatment conditions. The results show that the glass sintered at slow heating rate shows a slight increase in the density and microhardness, while the refraction index is almost invariant. Table 5 displays the comparison of the corresponding properties of the glass prepared by sol-gel method

Table 3 Composition and weight loss of Na₂O–B₂O₃–SiO₂ gel and glass

Sample	Sintering conditions	Chemical composition (mol%)	Ignition loss conditions	Ignition loss
Standardization composition	–	5Na ₂ O–20B ₂ O ₃ –75SiO ₂	–	–
Stiff gel	60–80 °C × 720 h	5.4Na ₂ O–19B ₂ O ₃ –75.5SiO ₂	180 °C/h 900 °C × 2 h	21.20%
Glass	700 °C × 12 h	5.74Na ₂ O–21.38B ₂ O ₃ –72.88SiO ₂		0.06%

Table 4 Properties of Na₂O–B₂O₃–SiO₂ glass

Sintering conditions	Density (g/cm ³)	Microhardness (kg/mm ²)	Refractive index
580 °C × 12 h × 10 °C/h	2.18	615	1.4762
600 °C × 24 h 300 °C × 5 h × 10 °C/h	2.21	620	1.4761
600 °C × 24 h × 10 °C/h	2.22	623	1.4759
700 °C × 24 h 300 °C × 5 h × 10 °C/h	2.26	673	1.4760

Table 5 Properties of gel-derived and melt-quenched glasses

Item	Gel-derived glass	Gel-derived glass	Melt-quenched glass
Composition mol%			
Normal (design)	5Na ₂ O–20B ₂ O ₃ –75SiO ₂	5.0Na ₂ O–25.0B ₂ O ₃ –70.0SiO ₂	5.7Na ₂ O–15.0B ₂ O ₃ –79.3SiO ₂
Dry gel	–	5.7Na ₂ O–14.6B ₂ O ₃ –79.7SiO ₂	–
Glass	5.74Na ₂ O–19.04B ₂ O ₃ –75.21SiO ₂	5.8Na ₂ O–12.4B ₂ O ₃ –81.4SiO ₂	5.8Na ₂ O–13.2B ₂ O ₃ –81.0SiO ₂
Density (g/cm ³)	2.26	2.27	2.24
Glass transition temperature (°C)	493	540	528
Thermal expansion coefficient (°C ⁻¹)	40–41 × 10 ⁻⁷	41 × 10 ⁻⁷	39–40 × 10 ⁻⁷
Chemical durability extracted Na ₂ O (wt%)	6–7	12–13	1–2

and melting method. In our design composition, the glass transition temperature is lower than others, and density and thermal expansion coefficient are similar.

The Structural Analysis of the Formation Process from Gel to Glass

TG-DTA analysis: The TG-DTA curves of the stiff gel are obtained under dynamic conditions in oxygen atmosphere from room temperature to 800 °C at a heating rate of 10 °C/min, as shown in Fig. 6a. The TG curve shows that the sample has a continuous

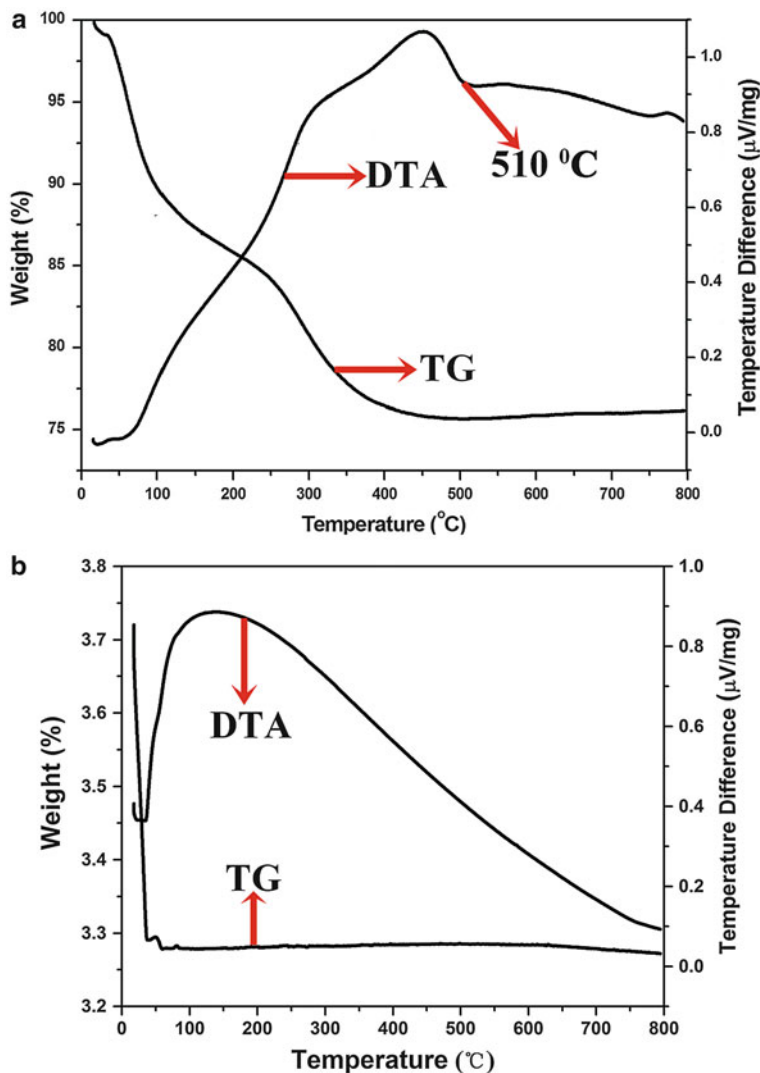


Fig. 6 (a) TG-DTA curves of the stiff gel sample; (b) TG-DTA curves of the glass sample

and obvious weight loss which is about 24% from room temperature to 400 °C. The weight loss at lower temperatures is mainly attributed to the release of water molecules, alcohols, and other organic solvents, while that which occurred at higher temperatures is mainly due to the decomposition of the organic ligands produced by the initial reaction. The DTA curve reveals that a broad exothermic peak in this temperature range is exothermic. As temperatures increase higher than 500 °C, the weight of the stiff gel becomes constant, and the DTA curve becomes flat. The DTA curve shows a broad endothermic peak at 500 °C due to the removal of the water and the organic

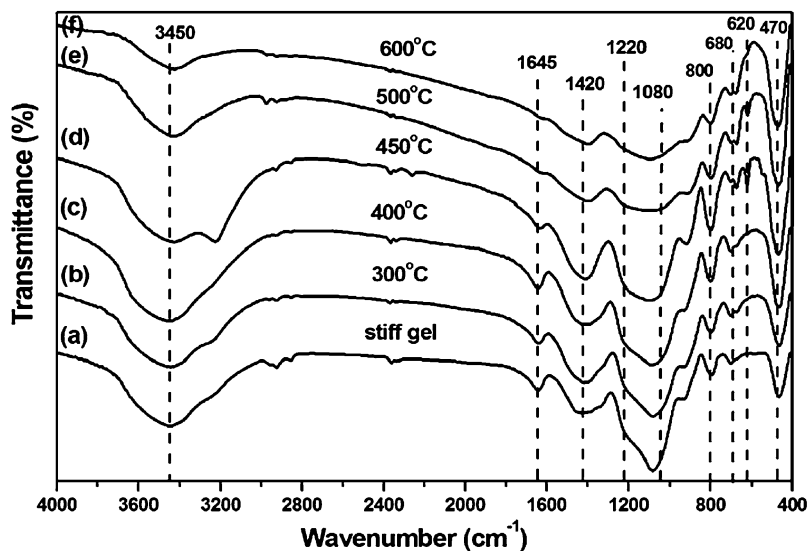


Fig. 7 FT-IR spectra of sodium borosilicate stiff gel: (a) stiff gel; (b) 300 °C; (c) 400 °C; (d) 450 °C; (e) 500 °C; (f) 600 °C

components. In addition, an absorbed heat peak at 510 °C is observed, which is considered the glass transition temperature T_g . In order to more accurately illustrate that the xerogel samples treated at 600 °C became glass, we also obtain the TG–DTA curve of the sample sintered at 600 °C. Figure 6b is the TG–DTA curve of the xerogel sample which is sintered at 600 °C, the TG curve shows the sample has no obvious weight loss in the whole heating range, and the DTA curve shows no endothermic peak either, suggesting that the sample sintered at 600 °C has become densified glass.

IR analysis: To get quantitative information about the structural groups as the processing temperature, the FT-IR spectra have to be measured. Figure 7 shows the FT-IR spectra of the dried gel heat-treated at different temperatures, as well as that referring to the glass of the same composition. The observed bands could be attributed to the vibrational band of specific groups. From Fig. 7, it can be noticed that the absorption bands appearing at about 3450 cm^{-1} can be assigned to water molecules, in which some of the OH group glass powder during measurements, and KBr absorbs moisture and remained in the disks (Marzouk et al. 2013; Rajesh et al. 2013). The band at 3000–2800 cm^{-1} originates from hydrogen bonding, and the band in the region of 2400–2300 cm^{-1} is due to the hydrogen-bonded OH-stretching vibrations (Saad et al. 2011). The band appearing at about 1645 cm^{-1} may be assigned to vibrations of water in these samples (Efimov and Pogareva 2000). The peak around 1420 cm^{-1} has been attributed to the stretching vibration of the B–O linkages present in various boron structural units (Muralidharan et al. 2004). The broad absorption bands observed in 1080 and 800 cm^{-1} are assigned to the combined stretching vibration of Si–O–Si and B–O–B tetrahedral network (Yusufali et al. 2013). The band at 1080 cm^{-1} is assigned to B–O bond vibration in BO_4 units and is also

associated with the stretching frequency of Si–O–B (Muralidharan et al. 2004). The band at 680 cm^{-1} is assigned to the bending vibrations of bridging oxygen (BO) between trigonal BO_3 groups. A broad band centered at 470 cm^{-1} corresponds to the Si–O–Si bending vibrations (Rao et al. 2013).

By comparing the spectra of the sample at different temperatures, it is found that a significant decrease of the absorption intensity of the shoulder appears at 3450 cm^{-1} . Especially, the band intensity presenting at 1645 cm^{-1} in the spectra highly decreases as the temperatures increase. These results are consistent with the TG curves. Furthermore, the Si–O–B vibration band which appears at 1080 cm^{-1} becomes more intense with increasing temperature, which could be indicative of the fact that the densifying gel gives rise to mixed Si–O–B links (Villegas and Fernandez Navarro 1988).

X-ray diffraction analysis: The NBS system xerogels are treated for 24 h in the temperature range of 300 to $750\text{ }^\circ\text{C}$ (heating rate $20\text{ }^\circ\text{C/h}$). The XRD patterns of the samples are shown in Fig. 8; no crystal diffraction peaks are found, suggesting the samples are in amorphous phase.

XPS analysis: The XPS spectra of Na 1s, B 1s, Si 2p, and O 1s are shown in Fig. 9. The peaks at 1071.8 eV in Fig. 9a correspond to the spectra of Na 1s electrons, which correspond to Na 1s of Na_2O (Nesbitt et al. 2011). The B 1s electron spectra (in Fig. 9b) show the characteristic binding energies at 192.7 eV , which confirms the formation of B_2O_3 (Hayashi et al. 2002). The Si 2p peak in Fig. 9c is observed at 103.2 eV , which is very close to that of standard SiO_2 (Si 2p, 103.3 eV) (Zhao et al. 2011), indicating that oxidized Si is in quadrivalent state. The peak of the O 1s electron spectrum in Fig. 9d is observed at 532.4 eV .

The $\text{Na}_2\text{O–B}_2\text{O}_3\text{–SiO}_2$ glass contains various chemical bondings such as Si–O–Si, Si–O– B_n , $\text{B}_n\text{–O–B}_n$ ($n = 3$ or 4 , n means the coordination number of

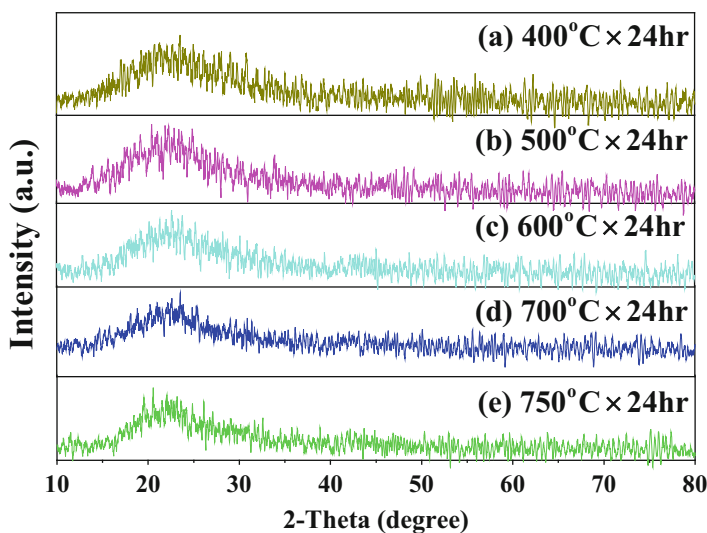


Fig. 8 The relationship of X-ray diffraction for a stiff gel with heat-treatment temperature

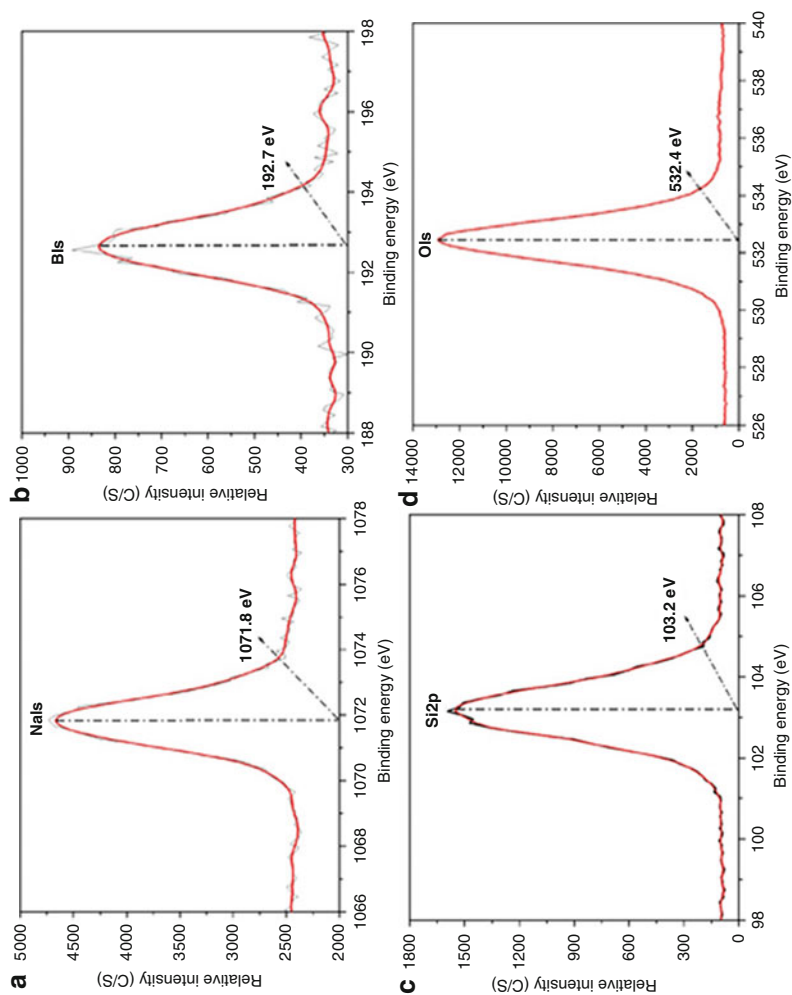


Fig. 9 XPS spectra of the glass: (a) Na 1s, (b) B 1s, (c) Si 2p, and (d) O 1s

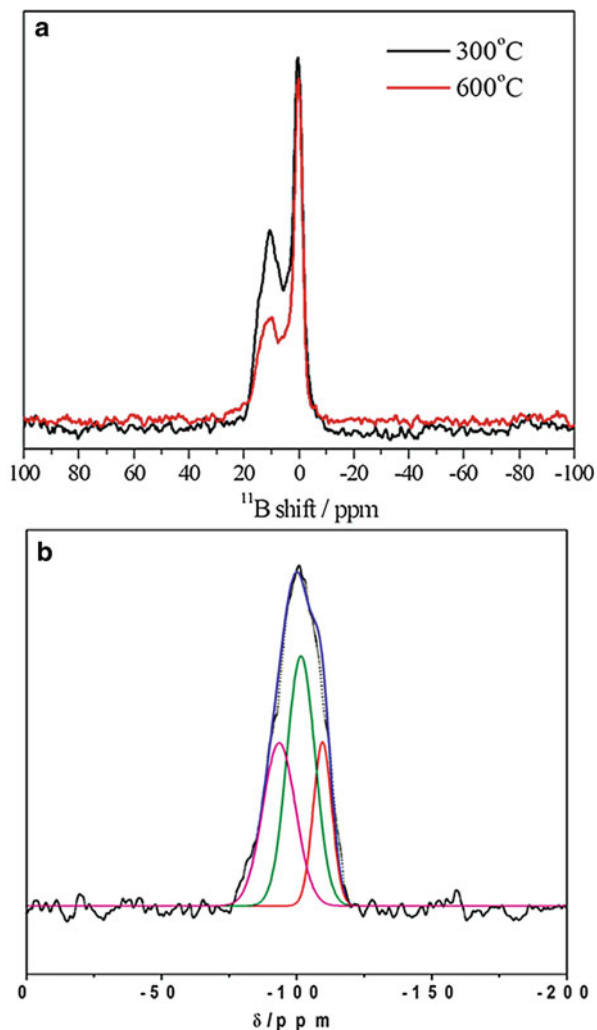
oxides around a boron atom) for the bridging oxygen (BO) component, and two types, Si–O – Na⁺ and B₃–O – Na⁺, for the non-bridging oxygen (NBO) component (Miura et al. 2001). The properties of glass are strongly dependent upon the average number of BOs in each Si–O polyhedron of glass. Considering the network structure and electrovalent balance in glass, the linking degree of the network becomes weak when the number of BOs decreases. Miura et al. (2001) have studied the Na₂O–B₂O₃–SiO₂ glass system by X-ray photoelectron spectrum and concluded that the number of NBOs should be very small in the glass composition (Yang et al. 2010). Therefore, the NBO component should be small in our system, and the amount of bridging oxygen bonds are formed in the glass. The linking degree of the glass network structure is strengthened with a large number of BO bonds, and the formation ability of glass is enhanced (Yang et al. 2010; Wu et al. 2013).

NMR analysis: As well as the vibrational spectroscopic work, the NMR investigation has been also particularly helpful in identifying various boron–oxygen arrangements at different modification levels in sodium borate glasses. By virtue of their distinctly different local symmetries, B(III) and B(IV) coordinations are readily distinguished by ¹¹B NMR. Figure 10a displays the ¹¹B NMR spectra of 5.74Na₂O–21.38B₂O₃–72.88SiO₂ glass heat treatment at 300 °C and 600 °C. The relatively broad resonances centered at around 10 ppm correspond to trigonal boron [BO₃] units, and the sharp signal near 0 ppm corresponds to the tetrahedral boron [BO₄] unit (Wu et al. 2013). The intensity corresponding to tetrahedral boron atoms is higher than the trigonal boron atoms. Bray et al. proposed that if the molar ratio Na₂O/B₂O₃ is less than 0.5 (in our experiment the value is ~0.3), the Na⁺ ions are attracted primarily by the borate network, and the oxygen atoms introduced by the Na₂O are used entirely to convert trigonal [BO₃] units to tetrahedral [BO₄] (Liu et al. 2008). From the curve (red line) in the spectra heat treated to 600 °C, it can be observe that the 10-ppm component decreases remarkably compared with the signal that appears in the spectra of the sample heated to 300 °C. A sum of contributions to the spectra is that a small fraction of the [BO₃] units converted into [BO₄] units as the heat treatment temperature increased from 300 °C to 600 °C. These results are in good agreement to that obtained from FT-IR and TG analyses.

The ²⁹Si NMR spectra indicate the existence of Si(OSi)₄, Si(OSi)₃OH, and Si(OSi)₂(OH)₂ groups, and the xerogel heat-treated at 600 °C changes into glass, proofed by the widened peak at –100 ppm, as shown in Fig. 10b.

The expansion curve of NBS glass: After dry gel changes into glass, the expansion coefficient curves are measured. Figure 11 showed that the expansion coefficient curve of NBS glass system prepared by sol-gel method is above the transition temperature T_g , and the change is small, and a linear relationship is very good before 350 °C. Particularly, above the transformation temperature, this expansion curve shape and the coefficient of expansion of tempered glass are very similar. Based on this, the determination of the second expansion coefficient curve above T_g for the expansion coefficient change rapidly increased and quickly reduced after softening point T_f , which show the typical shape of annealing glass expansion coefficient curve, $\bar{\alpha}_1 = 41 \times 10^{-17}/^\circ\text{C}$ and $\bar{\alpha}_2 = 40 \times 10^{-17}/^\circ\text{C}$ (Fig. 12).

Fig. 10 (a) ^{11}B NMR spectrum of sodium borosilicate stiff gel heat-treated in different temperatures; (b) ^{29}Si NMR spectrum of sodium borosilicate stiff gel heat-treated in 600 °C



The Common Hybrid Borosilicate Glass

Metal and Metal Oxide Nanoparticles Doped Borosilicate Glass

Since the first small pieces of transparent borosilicate glass prepared by sol-gel process by Dislich in 1971, many glass researchers tried to prepare and study bulk silica glasses and multicomponent glasses by sol-gel method (Sakka 2005). As the electronic density of states, quantum effect, and dielectric confinement endow metal nanoparticles unique and excellent optical, electrical, magnetic, chemical, and thermal properties (Speranza et al. 2009; Prasad 2004) and that metal or semiconductor

Fig. 11 Expansion coefficient plot of $\text{Na}_2\text{O}-\text{B}_2\text{O}_3-\text{SiO}_2$ glass prepared by sol-gel process (measured by second time $\bar{\alpha} = 41 \times 10^{-17}/^\circ\text{C}$)

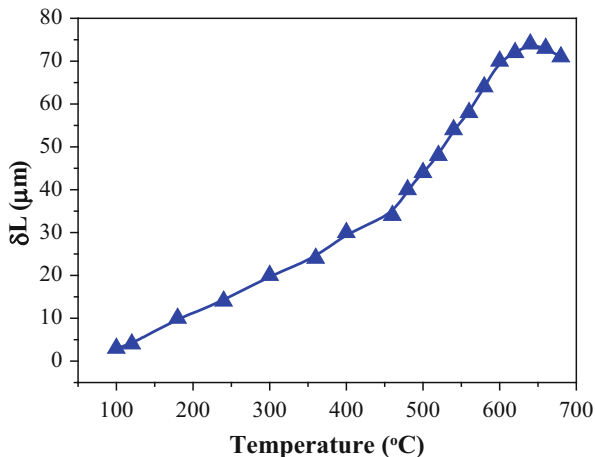
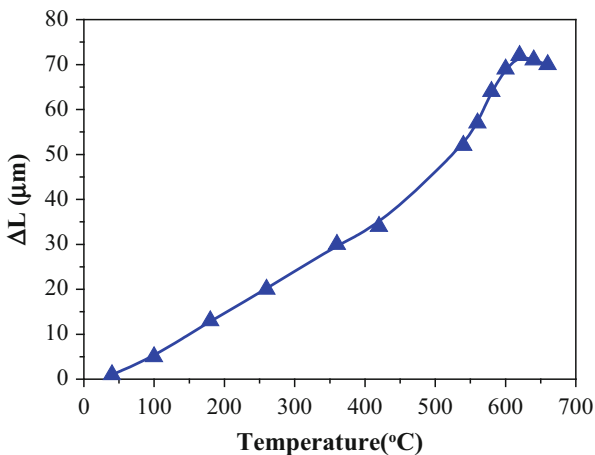


Fig. 12 Expansion coefficient plot of $\text{Na}_2\text{O}-\text{B}_2\text{O}_3-\text{SiO}_2$ glass prepared by sol-gel process (measured by second time $\bar{\alpha} = 40 \times 10^{-17}/^\circ\text{C}$)



nanoclusters dispersed in a transparent matrix, such as glass, can exhibit unique and excellent properties compared to the bulk metal material, more and more researchers are focusing on the facile synthesis of metal or metal oxide nanoparticles hybrid materials. Nanometallic glass composites have attracted researchers' great attention, not only because they can be applied to photochromic materials, colored glass circulation industry, and three-dimensional color crafts but also because of their great potential applications in optical materials (Korgel 2013; Chen et al. 2001; Zeng et al. 2004; Mangin et al. 2014; Llordés et al. 2013). In all these applications, the particle size, shape, number density, and distribution of nanoparticles together determine the characteristics and performance of the nanometer composite materials. Borosilicate glass prepared by sol-gel and heat treatment method undergoes the phase change of solution-xerogel-glass, during which chemicals can be easily

doped and well dispersed, porous structure can be naturally formed, and substances doped can be well encapsulated and preserved. Therefore, borosilicate glass is a competent host glass to load and encapsulate metal nanoparticles.

S. Tamil Selvan et al (2002) prepared sol-gel-derived gold nanoclusters in silica glass for potential photonic applications. M. Epifani et al. (2001) prepared bulk borosilicate glasses (with nominal molar composition of 10% B_2O_3 –90% SiO_2) doped with gold nanoparticles by sol-gel process and found that Au particles have two patterns of existence form: face-centered cubic Au and orthorhombic Au_3Si .

Xiang et al. have been devoted in the solution–gel–glass transition process, metal, and metal oxide (e.g., Au (2015), Ag (2014), Cu (2015), Pb (2014), Sb (2014), Bi (2011), In (2012), Cu_2O (2015), CuO (2015), Bi_2O_3 (2011), Zhang et al. (2014) etc.) nanoparticles doped monolithic sodium borosilicate glasses by sol-gel route. The detailed process of sol-gel preparation of Au nanocrystals doped monolithic, and transparent sodium borosilicate glass (Gao et al. 2015) was shown in Fig. 13.

The preparation of uniform spherical-shaped Ag nanocrystals doped sodium borosilicate monolithic transparent glass by sol-gel method is described (Pei et al. 2014). The XRD patterns and absorption spectra of the Ag doped NBS glass is shown in Figs. 14 and 15. The XRD patterns showed that with increasing the heat treatment temperature from 420 °C to 470 °C, the full width at half maximum gradually broadened, indicating that microcrystalline dimension of Ag nanocrystals can be controlled by the heated treatment. Surface plasma resonance absorption peaks of the Ag nanocrystal glass at about 406 nm are obtained, and their intensity is changed with different heat treatment temperatures.

Additionally, clearly seen from Fig. 16 is the pore shrinking with increasing of the sintering temperature. The pore size distribution obtained by the BJH method of sample at 420 °C, 450 °C, and 470 °C are centered at 3.34, 2.35, and 2.17 nm, respectively. The reason is that the glass transition temperature T_g of NBS glass matrix is about 565 °C, so the sample has been densified at 600 °C.

Of all the metal element doped glasses, the effective valence control of metal nanoparticles doped in the borosilicate glass is especially interesting and of scientific research value. Take copper, for example, as an important transition metal element, copper has a face-centered cubic crystal system, with the lattice constant of $a = b = c$ and $\alpha = \beta = \gamma = 90^\circ$. The valence shell structure of Cu is $3d^{10}4s^1$; therefore, the valence of Cu can exhibit 0, +1, and +2; nevertheless, controlling the chemical valence state of Cu freely in the glass is still very challenging, especially the +1 of Cu. A detailed study (Xiang et al. 2015) was carried out, from synthesis to characterization, on the valence state control of copper in sodium borosilicate glass synthesized by the sol-gel process and different atmosphere control heat treatment. The glass samples are shown in Fig. 17a–c; the diameter of which are about 1 cm. X-ray diffraction analysis of the well-cut and polished glasses is performed to explore whether the crystalline structure has formed in the glass. Figure 17d shows the XRD pattern of glass samples. Besides the bag-like amorphous peak while 2θ was about 22° which is caused by the base glass diffraction. The red glass has three sharp peaks which are in good accordance with the standard card JCPDS no.04-0836, indicating that pure Cu crystals have formed in the red glass. The green

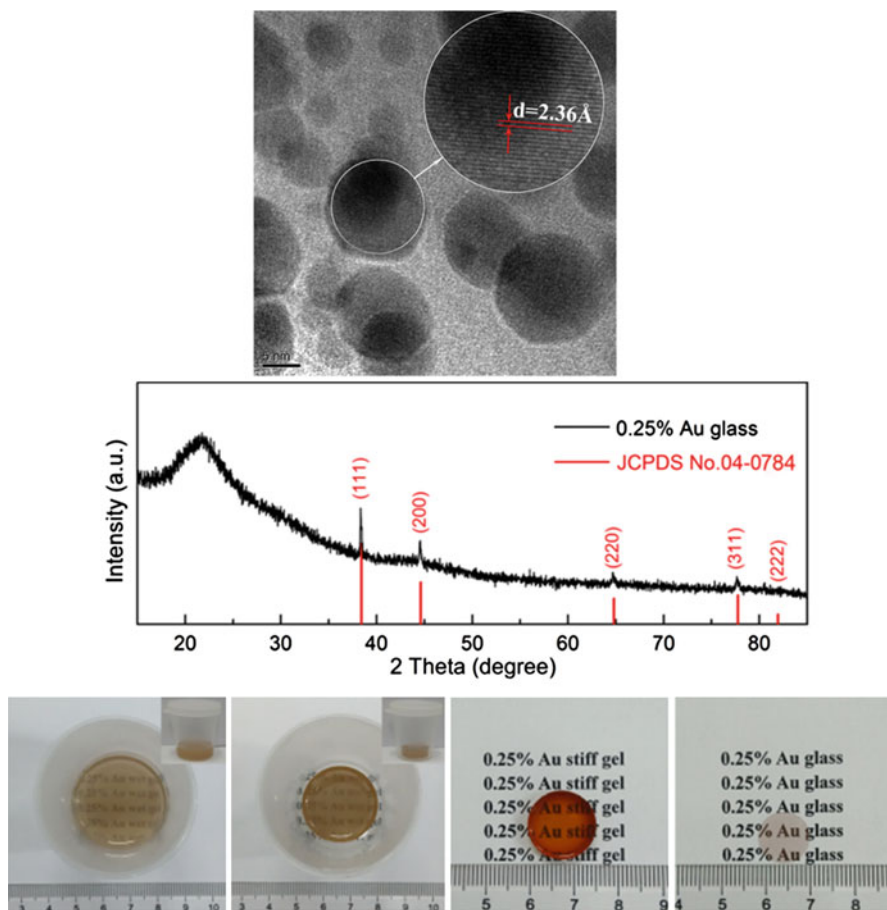


Fig. 13 The HRTEM image of Au nanoparticles, XRD pattern of the Au nanoparticles doped glass, and photos of samples in the preparation procedure

curve and the blue curve have no signals of diffraction peak except the big bag-like amorphous peak; the reason could be that the crystals formed are too small to lead to agglomeration, causing diffraction peaks broadening and being not obvious.

To essentially and precisely find out the truth, the following TEM is applied to insight into the inner structure of the glass. Figure 18a–c show the TEM images of the red, green, and blue glasses. Lots of black particles with different sizes embedded in each of the glass substrate. HRTEM images in Fig. 18d–f show the HRTEM images of NPs in red, green, and blue glasses, and the lattice parameters are measured to be 2.09 Å, 2.12 Å, and 2.14 Å, very close to pure Cu metal (JCPDS#04-0836, 2.088 Å for [111] plane), Cu_2O (JCPDS#34-1354, 2.120 Å for [200] plane), and CuO (JCPDS#44-0706, 2.140 Å for [200] plane), respectively.

As the XPS analysis is not sure to confirm the valence state of copper in the three glasses, electron energy loss spectroscopy is applied subsequently. Figure 19a is the

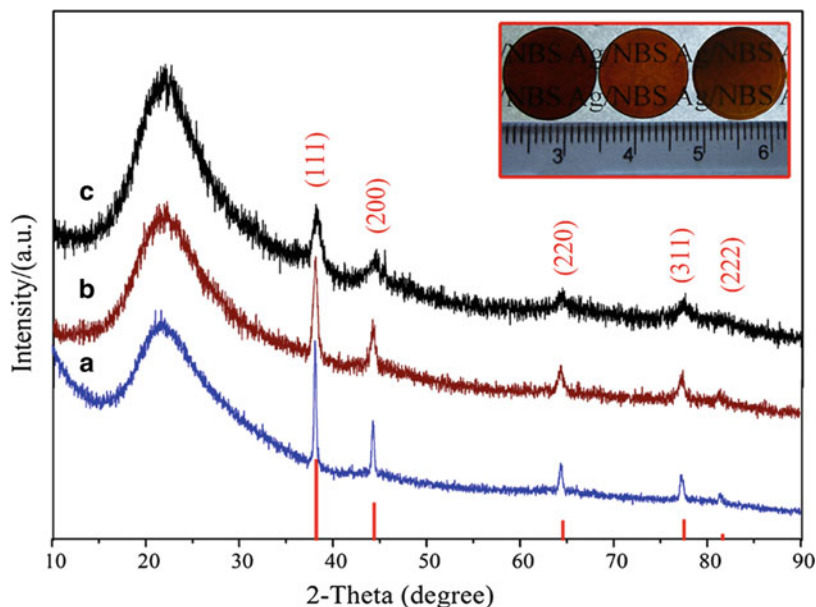


Fig. 14 XRD patterns of the Ag doped NBS glasses obtained after sintering at (a) 420 °C, (b) 45 °C, and (c) 470 °C. *Inset* shows the as obtained samples

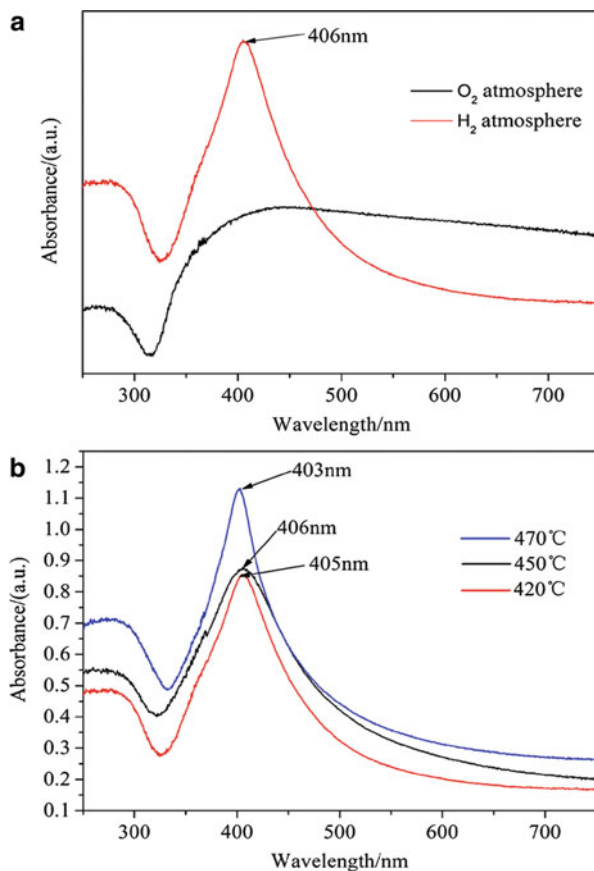
high-angle annular dark-field (HAADF) image of the red glass; Fig. 19b representing 3D view of the result of EELS line scan from A to B proves that the NPs in NBS glass are Cu-rich particles.

The EELS spectrum of NPs in red, green, and blue glasses shows in red, green, and blue lines in Fig. 20b, and the EELS spectra of reference Cu, Cu₂O, and CuO are shown in Fig. 20a. It is found that the valence of Cu ions in green and blue glasses is not only +1 and +2, respectively, which may be a bit of Cu⁺ in blue glass and Cu²⁺ in green glass. Combined with XRD, HRTEM, and XPS analysis, the main NPs in the red, green, and blue glasses should be Cu, Cu₂O, and CuO nanoparticles, respectively.

Open aperture (OA) and closed aperture (CA) Z-scan measurements are carried out to determine the nonlinear refraction and absorption of the copper doped sodium borosilicate glass samples. Figure 21 represents open-aperture ($S = 1$) and closed-aperture ($S = 0.05$) Z-scan results with single-pulse energy of 0.36 μJ for Na₂O–B₂O₃–SiO₂ glass containing Cu, Cu₂O, and CuO NPs, respectively.

All of the nonlinear parameters are listed in Table 6. Obviously, the introduction of Cu, Cu₂O, and CuO nanocrystals in sodium borosilicate glass would result in different third-order nonlinear properties of the glass. For example, when Cu⁰ presents in the glass, the third-order nonlinear absorption is reverse saturable and the third-order nonlinear susceptibility is as high as 6.4×10^{-14} esu, which is the maximum of the three glass samples. While Cu²⁺ is doped in the glass, it turns out to be of saturable absorption and the third-order nonlinear susceptibility reaches 1.6×10^{-14} esu.

Fig. 15 The absorption spectra of the Ag doped NBS glass. **(a)** Effects of different atmospheres on the absorption spectra of samples. **(b)** Effects of different heat temperatures on absorption spectra of samples



Besides, Yang et al. (2011) reported a facile method to realize the fabrication of $Na_2O-B_2O_3-SiO_2$ glass containing metallic Bi and Bi_2O_3 crystals; the XRD patterns of the samples are shown in Fig. 22.

Figure 23a–b represent the morphological features of the glasses containing metallic Bi and Bi_2O_3 crystals. It is clear that some black nanometer-sized particles are mounted uniformly in the glass matrix, among which these particles are spherical in shape. Energy-dispersive X-ray (EDX) spectra (Fig. 23c, d) and high-resolution TEM (HRTEM) analysis (Fig. 23e, f) are further performed to confirm the chemical compositions and crystalline structures of these black nanometer-sized particles.

The third-order nonlinear optical properties of the samples are tested by Z-scan technique. The OA Z-scan results for glass sample containing metallic Bi and Bi_2O_3 . Both the two OA Z-scan models show an obvious enhanced transmittance near the focus ($z = 0$) in the two glasses, occurring due to saturable absorption. Interestingly, the CA Z-scan results for glasses containing metallic Bi and Bi_2O_3 crystals display self-focusing and self-defocusing nonlinear refractive process, respectively.

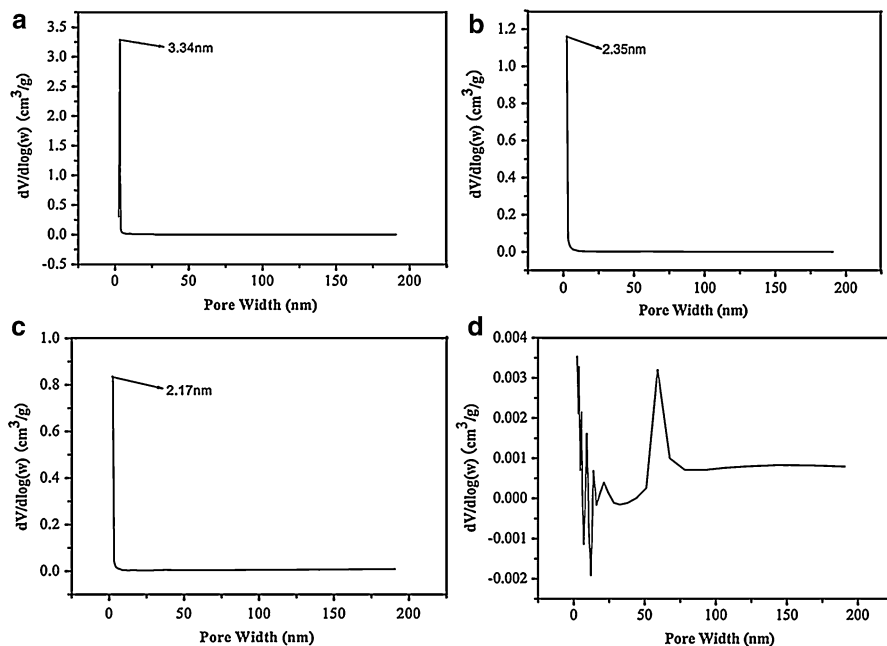


Fig. 16 BJH pore-size distribution curves of Ag doped NBS glass stabilized at (a) 420 °C, (b) 450 °C, (c) 470 °C, and (d) 600 °C

The adjustment of nonlinear absorption of the copper doped sodium borosilicate glass from reverse saturable absorption to saturable absorption in the single-pulse energy range of 0.36 to 1.5 μJ is realized when controlling the valence state of copper was realized. And the nonlinear refractive process of the sodium borosilicate glass is converted from self-focusing to self-defocusing by the doping of metallic Bi and Bi_2O_3 crystals. Therefore, the metal elements doped borosilicate glasses show interesting optical phenomenon; with further improvement, they may have potential applications in the field of nonlinear optics.

Nanoalloy Quantum Dots Doped Glass

Recently, considerable efforts have been devoted to bimetallic alloy nanoparticles, since they are of great interest from both scientific and technological perspective for the modification of physical and chemical properties of metal nanoparticles. Bimetallic alloy nanoparticles are more attractive over monometallic nanoparticles because they exhibit improved electronic, optical, and catalytic properties.

Zhong et al. (2013) synthesize borosilicate glasses doped Cu_2In alloy nanoparticles with hexagonal structure which are well distributed in the glass matrix. The crystal structure and phase composition of as-prepared glass are characterized

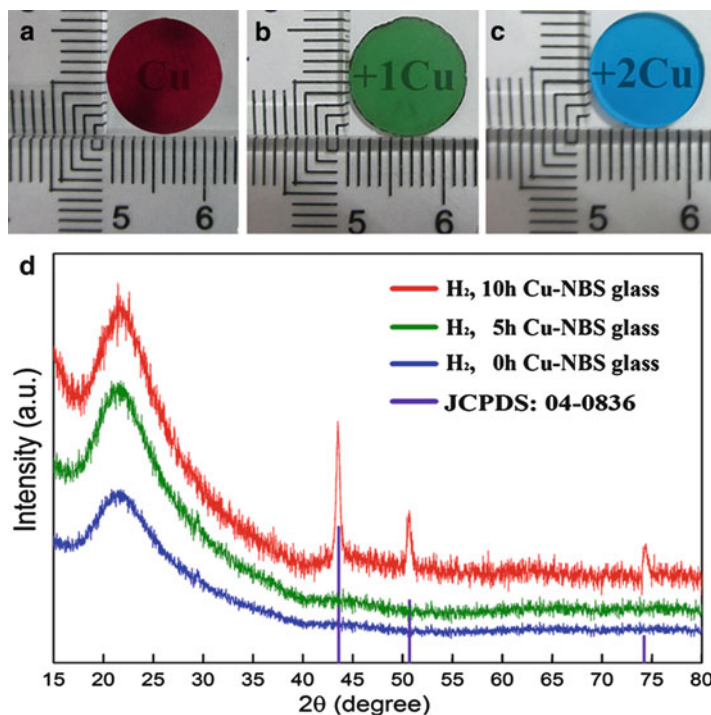


Fig. 17 The photograph of as-obtained glass, (a) red glass, (b) green glass, and (c) blue glass; (d) The XRD pattern of the glass

by XRD (Fig. 24). All diffraction peaks can be indexed to the hexagonal structure Cu_2In (JCPDS No.42-1475).

The internal morphology of the synthesized glass is investigated by using TEM. As shown in Fig. 25, TEM analysis shows that the Cu_2In nanoparticles are spherical shaped and highly monodispersed with an average size of about 30.28 nm.

Because of well-dispersed Cu_2In nanoparticles, the glass shows excellent third-order optical properties investigated at 800 nm by using femtosecond Z-scan measurements. The nonlinear refraction indices of these nanoparticles are measured in order of 10^{-16} m^2/W with negative sign, and the nonlinear absorption coefficients are obtained in order of 10^{-10} m/W with positive sign.

Not only that, Yin et al. (2014) reported on the synthesis of microstructure sodium borosilicate glass hybrid nanocomposites containing metallic Ag–Ga nanocrystals with a molar ratio of 1:1 (in Fig. 26) using similar methods. X-ray powder diffraction characteristic peaks in Fig. 27 show that the final glass should be a solid solution. It means that gallium element enters into the crystal lattice of silver element, causing a crystal distortion. TEM analysis indicates that the metallic Ag–Ga nanocrystals with spherical shape and a statistical average for the diameter of 25.0 nm have small size, narrow distribution, good dispersed form, and cubic phase in sodium borosilicate

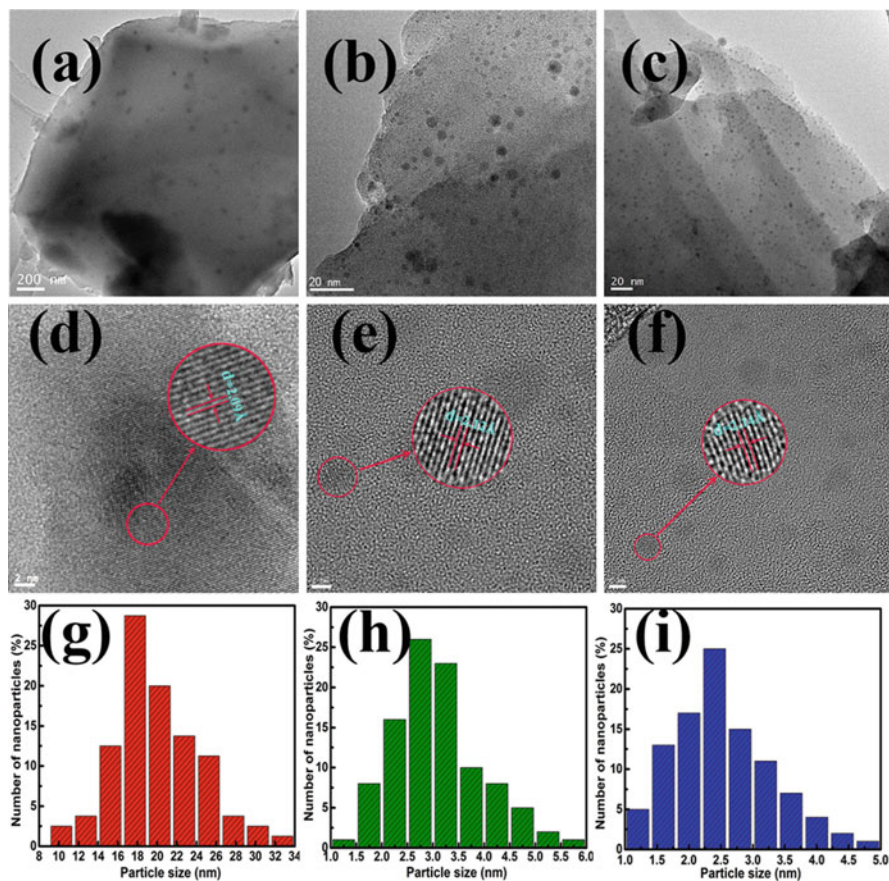


Fig. 18 TEM images of the glass samples: (a) red, (b) green, (c) blue; HRTEM images of the glass samples: (d) red, (e) green, (f) blue; Size-distribution images of (g) red, (h) green, and (i) blue glasses, respectively

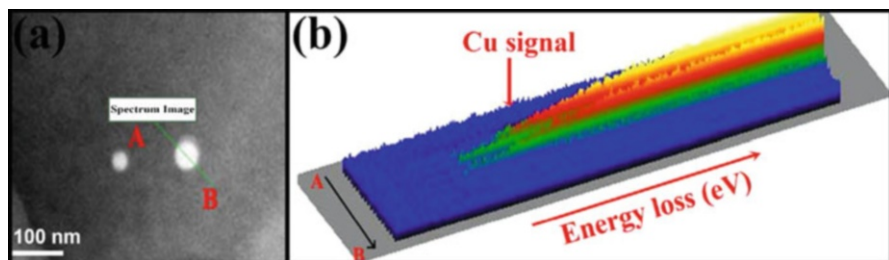


Fig. 19 (a) HAADF STEM image of the red glass. The line from A to B shows EELS line-scan direction. (b) 3D view of the EELS line-scan result

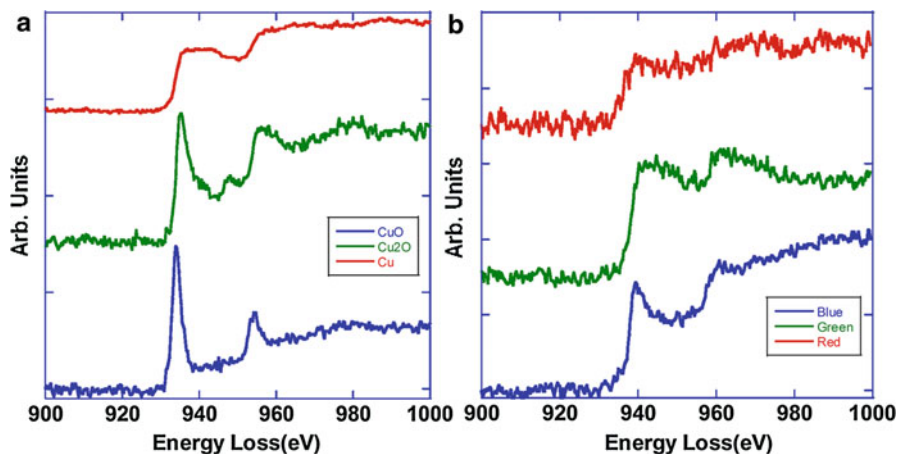


Fig. 20 (a) The reference EELS spectra of Cu; (b) The experimental EELS spectra reproduced from Fig. 17 (a-c)

glass. The final glass exhibits an enhanced photoluminescence (PL) intensity compared to stiff gel, which was ascribed to the surface plasmon resonance of metallic Ag–Ga nanocrystals.

Sulfide Quantum Dots Doped Glass

Semiconductor nanomaterials with great third-order optical nonlinearities and fast response times are important for future optical device applications. Among these semiconductor nanomaterials that have been studied in the field of nonlinear optics, the semiconductor quantum dots borosilicate glasses are regarded as an important kind of nonlinear optical material. Recently, many researchers have attempted to introduce various semiconductor quantum dots into the borosilicate glass matrices.

Xiang et al. (2012) reported CuInS_2 quantum dots doped sodium borosilicate glass is prepared by using both sol-gel and atmosphere control methods. The composition of the sodium borosilicate glass matrix was obtained $5.74\text{Na}_2\text{O}-21.38\text{B}_2\text{O}_3-72.88\text{SiO}_2$ (in wt%), and methanol solution containing cupric nitrate $[\text{Cu}(\text{NO}_3)_2 \cdot 3\text{H}_2\text{O}]$ and indium nitrate $[\text{In}(\text{NO}_3)_3]$ was added to the glass matrix to produce the CuInS_2 quantum dots. The resultant glass (Fig. 28) is obtained by exposing to dry hydrogen (H_2S) at 450°C for 10 h.

The crystalline structure of the CuInS_2 quantum dots in the glass is characterized through XRD analysis, as shown in Fig. 29. The CuInS_2 pattern of the Joint Committee on Powder Diffraction Standards (JCPDS) is shown for comparison. All of the diffraction peaks are indexed from the tetragonal phase of CuInS_2 (JCPDS-65-2732). No peak from any other phase is detected, indicating that pure CuInS_2 crystals have formed in the glass.

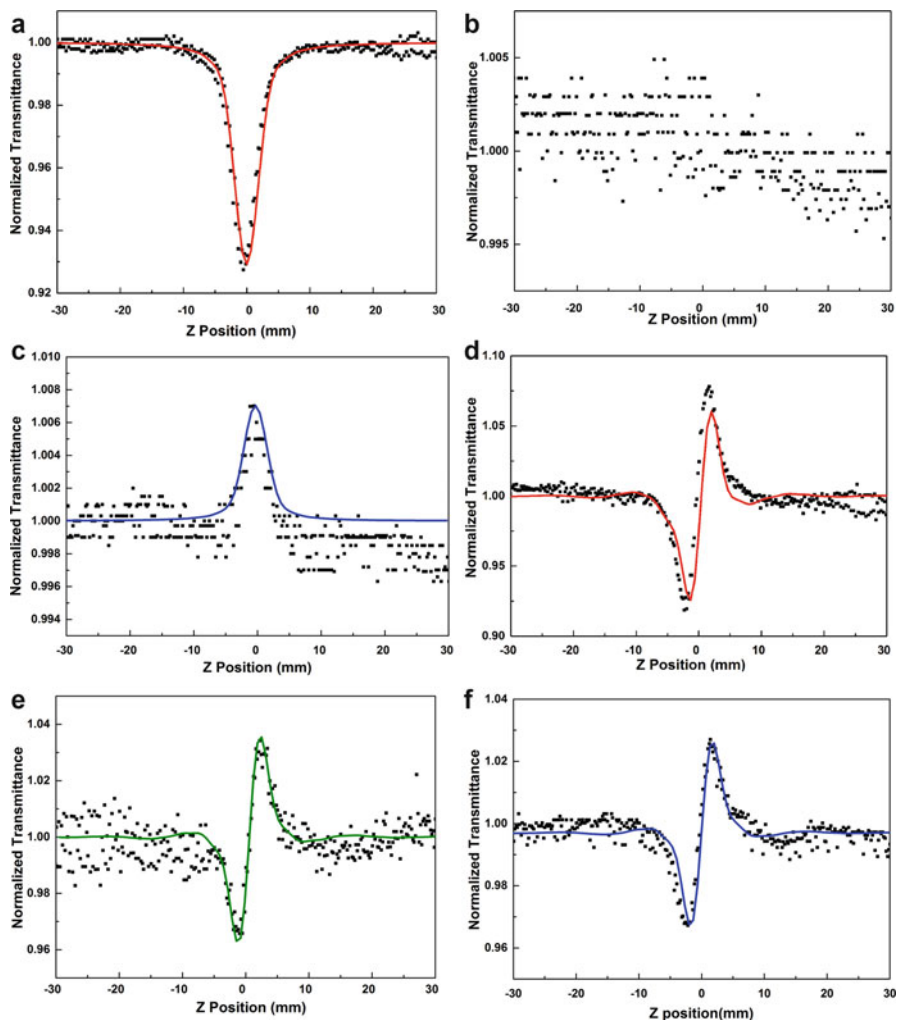


Fig. 21 The Z-scan normalized transmittance curves of the glasses with single-pulse energy of 0.36 μJ : (a) open-aperture Z-scan curve of the red glass; (b) open-aperture Z-scan curve of the green glass; (c) open-aperture Z-scan curve of the blue glass; (d) closed-aperture Z-scan curve of the red glass; (e) closed-aperture Z-scan curve of the green glass; (f) closed-aperture Z-scan curve of the blue glass (Theoretical data in *black squares* and fitting curves in *solid line*)

Table 6 The third-order nonlinear optical parameters of the three glasses at 800 nm (Xiang et al. 2015)

Parameters	$\gamma(\text{m}^2/\text{w})$	$\text{Re}\chi^{(3)}(\text{esu})$	$\beta(\text{m}/\text{w})$	$\text{Im}\chi^{(3)}(\text{esu})$	$\chi^{(3)}(\text{esu})$
Cu^0	5.3×10^{-20}	2.9×10^{-14}	4.1×10^{-13}	5.7×10^{-14}	6.4×10^{-14}
Cu^{1+}	2.9×10^{-20}	1.6×10^{-14}	0	0	1.6×10^{-14}
Cu^{2+}	4.2×10^{-20}	2.3×10^{-14}	-8.0×10^{-14}	1.1×10^{-14}	2.6×10^{-14}

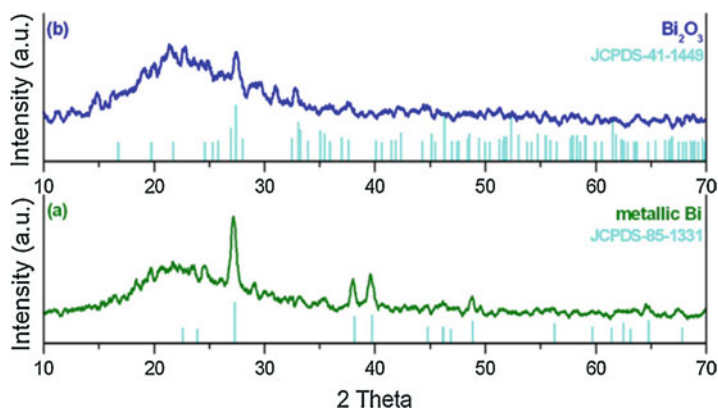


Fig. 22 XRD patterns of the glasses containing the various kinds of bismuth crystals: (a) metallic Bi, (b) Bi₂O₃. The JCPDS patterns of metallic Bi and Bi₂O₃ are also shown

The microstructure of the glass is examined using TEM as shown in Fig. 30. The results reveal that CuInS₂ quantum dots in a tetragonal crystal system have formed uniformly in the glass, and the size distribution of these quantum dots generally range from 5 to 15 nm.

The as-obtained semiconductor quantum dot glasses exhibit excellent nonlinear optical properties. The third-order optical nonlinear susceptibility of the glass doped with CuInS₂ quantum dots are five orders of magnitude larger than the un-doped glass. This result indicates that the introduction of the CuInS₂ quantum dots will contribute to the enhancement of the third-order nonlinear properties.

Likewise, Zhong et al. (2014) reported I–III–VI ternary semiconductor CuGaS₂ quantum dots embedded in sodium borosilicate glass matrix (Fig. 31) using sol-gel methods. The structure and morphology of the obtained glass are studied by using XRD and TEM. The results show that tetragonal crystalline phase of CuGaS₂ quantum dots with spherical shape is formed uniformly in the sodium borosilicate glass matrix, and the sizes range from 5 to 25 nm with an average particle size of 12.75 nm.

In addition to ternary sulfide quantum dots, a series of binary sulfide quantum dots such as Cu_{7.2}S₄, Bi₂S₃, and In₂S₃ (Zhao et al. 2012; Yang et al. 2011; Xiang et al. 2013) are also introduced in sodium borosilicate glass via sol-gel methods as shown in Fig. 32. The synthetic process of the glass is similar to previous CuInS₂ quantum dots doped glass, apart from employing different precursors. The microstructures of the glasses are investigated in detail by means of XRD, XPS, and TEM techniques. The results show these quantum dots have formed uniformly in the glass, but the size of these quantum dots are a little different. These transparent glasses all displayed excellent third-order nonlinear optical properties, which is attributed to cause obvious quantum confinement effects caused by the high-dispersion quantum dots. Among which, the orthorhombic Bi₂S₃ nanocrystals doped sodium borosilicate glasses range from 10 to 30 nm; the third-order nonlinear optical properties of the

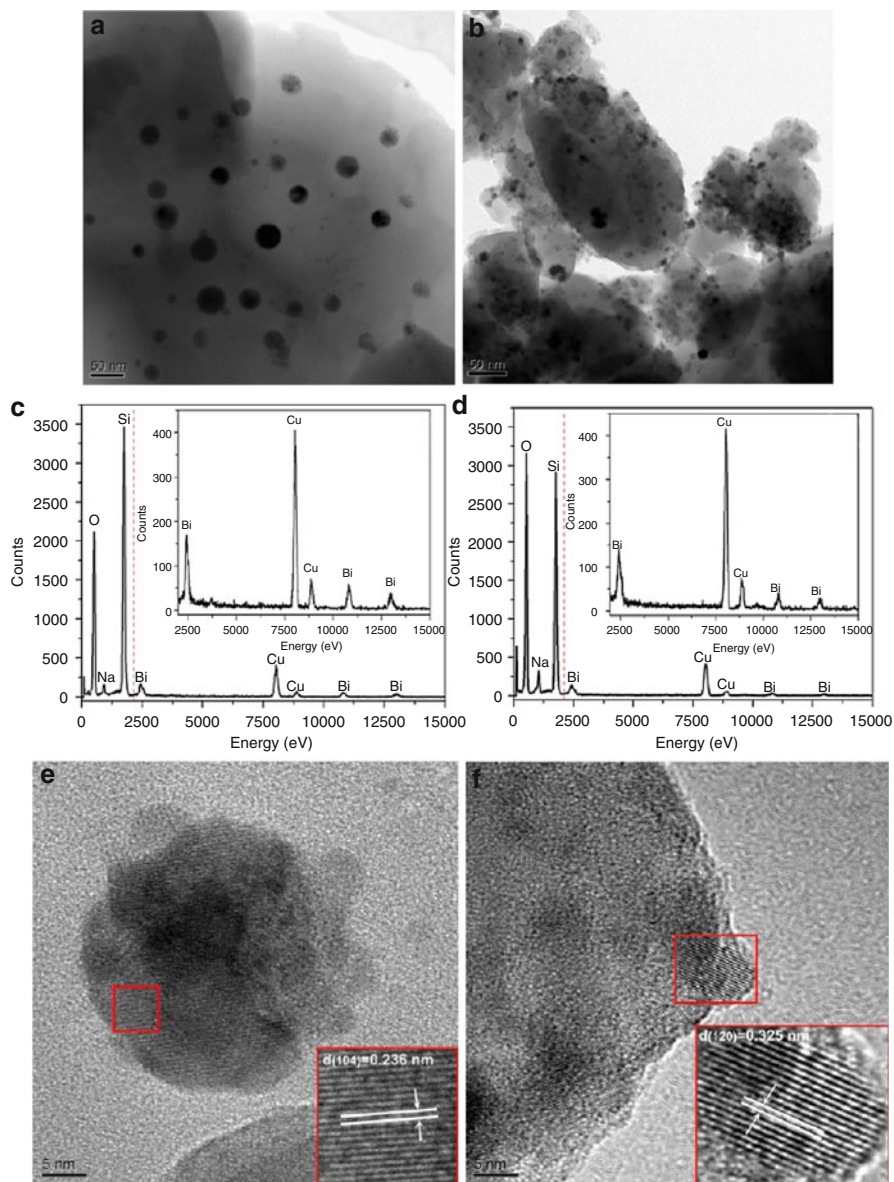


Fig. 23 TEM analysis of the Bi and Bi_2O_3 glasses: (a, b) morphological images; (c, d) EDX spectra; (e, f) HRTEM images

glass are measured by Z-scan technique at the wavelength of 770 nm; and the results show that the third-order nonlinear optical properties increased with the increase of the Bi_2S_3 content.

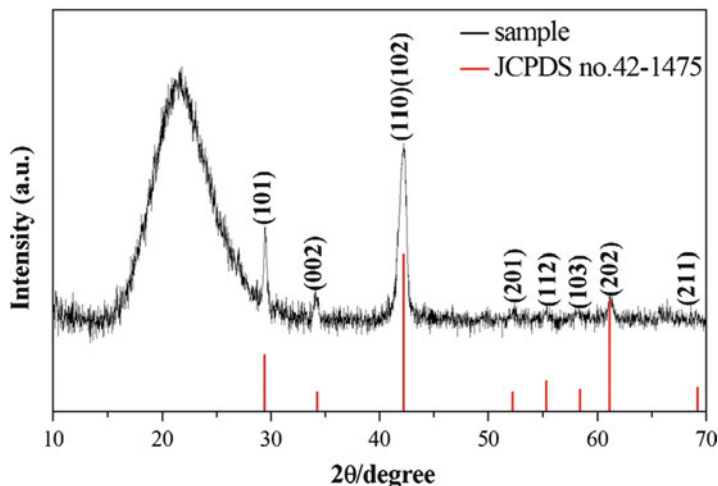


Fig. 24 XRD patterns of the as-prepared Cu_2In glass

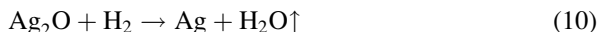
Formation Mechanism of Nanocrystals in Borosilicate Glass

What is more, the possible formation mechanism of some nanocrystals in borosilicate glass is proposed. Take Ag nanocrystals, for example; the formation mechanism is depicted from stage I to stage IV shown in the model in Fig. 33 (Pei et al. 2014).

In stage I, the hydrolysis, polycondensation, and aging of NBS precursors occurred successfully, leading to the dispersion of the Ag precursor (AgNO_3) in the NBS stiff gel system (see stage I in the model). After heated in tube furnace in oxygen (O_2) atmosphere, the loose and porous NBS xerogel could form due to organic substances being removed; meanwhile, the silver nitrate could be decomposed to Ag_2O , as shown in the stage II.



After the stage II, the xerogel undergoes heat treatment in dry hydrogen (H_2) atmosphere. With increasing of the treatment temperature, Ag_2O dispersed in mesoporous xerogel easily reacts with H_2 gas; the following reaction would occur; and the size of the as-formed Ag nanosphere is very small:



Further prolonging the reduction time can result in the growth of the primary Ag nanosphere. Therefore, Ag quantum dots with different sizes can be controlled by varying the reaction time. As the content of $[\text{Ag}]$ was kept at a constant value, increasing the reduction temperature in reducing atmosphere, due to the pore shrinking, the size of as-formed primary Ag nanocrystals decreases and the aggregation of Ag nanosphere could be suppressed, which is consistent with XRD

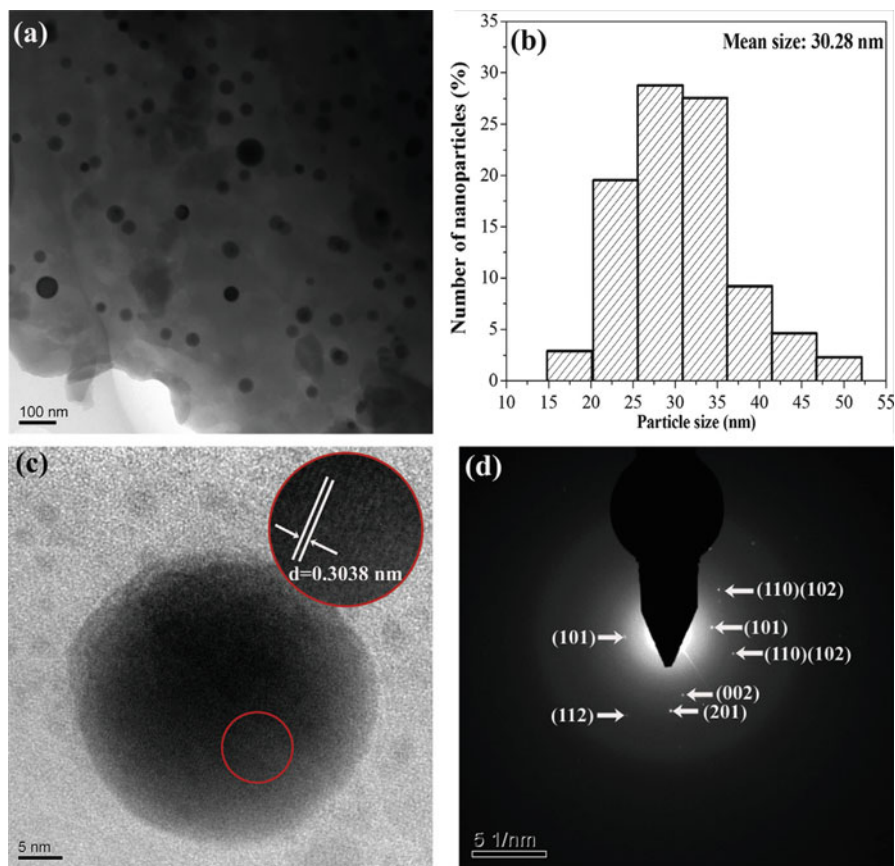


Fig. 25 (a and b) Representative TEM and size-distribution images for Cu_2In nanoparticles embedded in $\text{Na}_2\text{O}-\text{B}_2\text{O}_3-\text{SiO}_2$ glass, (c) HRTEM micrograph and (d) the corresponding SAED patterns for the same sample

observations (Fig. 14). In the stage III, the interconnected pores are continuing to contract, and this leads to the formation of a microporous space network frame structure of sodium borosilicate xerogel matrix.

After the stage III, the xerogel was sintered in nitrogen (N_2) atmosphere to 600°C to reach full densification. Finally, the crack-free monoliths sodium borosilicate glasses containing Ag nanocrystals are obtained with good transparency and mechanical strength (see stage IV in the model).

Organic Compounds Quantum Dots Doped Glass

Borosilicate glasses are widely employed in the chemical industry for their chemical resistance and low thermal expansion. Although monolithic borosilicate glasses

Fig. 26 Photograph of the as-obtained Ag–Ga samples (a) stiff gel; (b) final glass

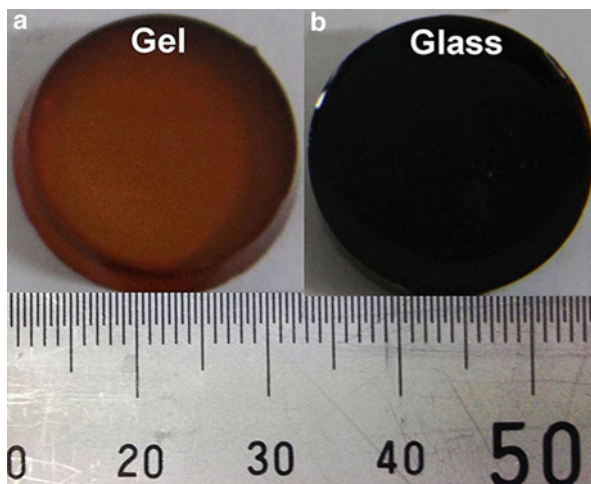
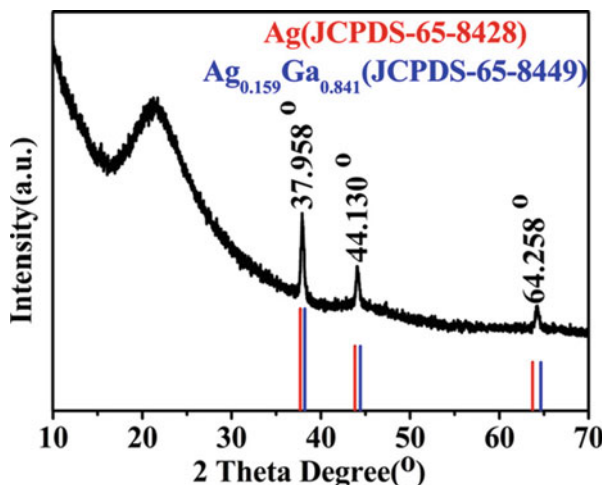


Fig. 27 X-ray powder diffraction pattern of Ag–Ga glass



generally possess a high elastic modulus and high density, they cannot be employed in several structural applications mainly due to their brittleness. Since the amorphous structure does not provide any obstacle to the fracture propagation (Boccaccini et al. 2005), sol-gel preparation of borosilicate glass compositions are difficult to achieve as the borosiloxane bonds are easily broken by hydrolysis. Irwin et al. (1987) and (1988) reported that only a few of borosiloxane bonds were present at gelation; the majority of the boron being in the form of boric acid. Formation of Si–O–B bonds in the gel can be promoted by using modified silicon alkoxide precursors such as $R_x\text{-Si(OR)}_{4-x}$, where $x = 1, 2, 3$ and R– is an organic group (Soraru et al. 1999; 2000). It has been suggested that the introduction of organic

Fig. 28 The image of the glass doped CuInS_2 quantum dots

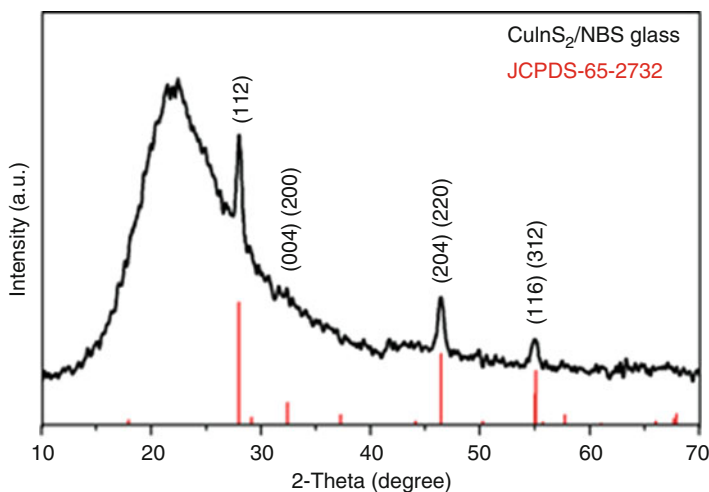
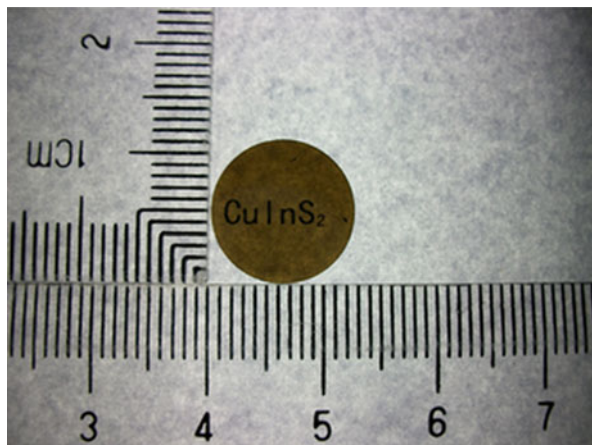


Fig. 29 Typical XRD pattern of the as-prepared glass doped CuInS_2 quantum dots

groups leads to a more hydrophobic siloxane network, favoring the removal of water and thus preventing hydrolysis of borosiloxane bonds.

Organic compounds are in the range of the promising reinforcing materials for structural composites. The reinforcement of glasses with carbon fibers has been found to be successful since the late 1960s (Crivelli-Visconti and Cooper 1969). Carbon fibers are very effective since the interface allows the load transfer between the phases, thus allowing a notable amount of energy to be dissipated during fracture propagation, due to debonding and pullout of the fibers. The fracture toughness of carbon fiber-reinforced glass matrix composites may reach excellent values

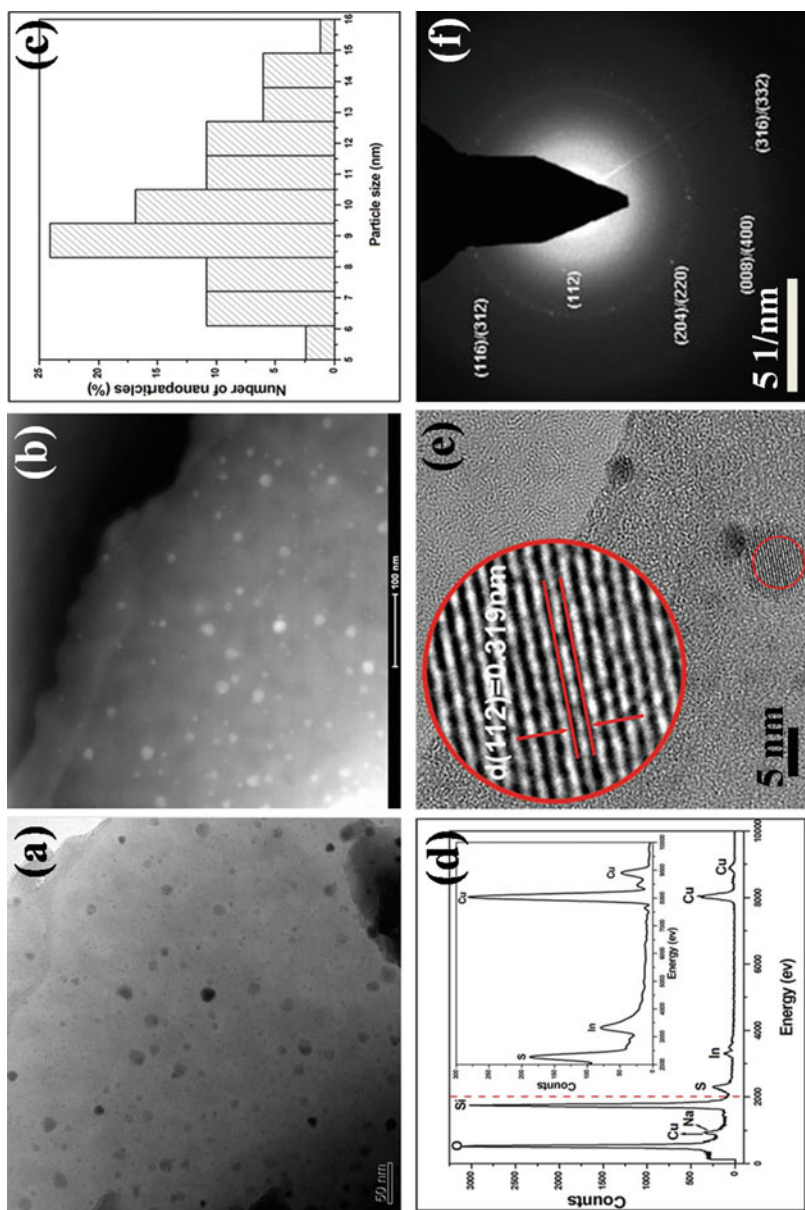


Fig. 30 TEM images of the glass doped CuInS₂ quantum dots

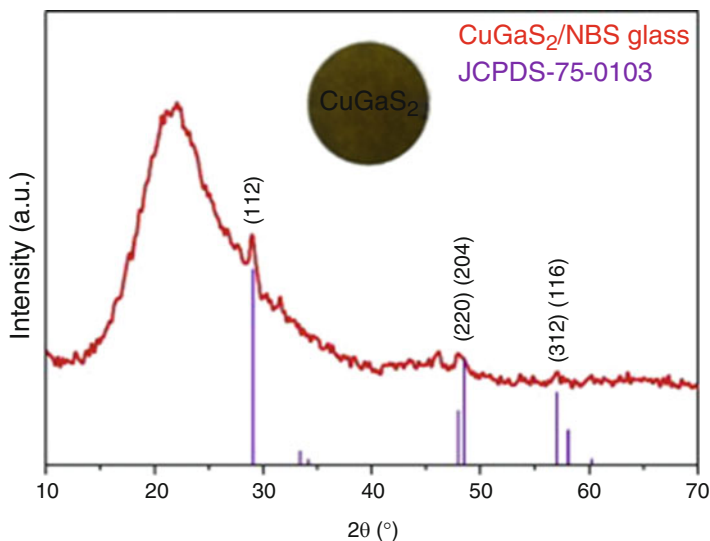
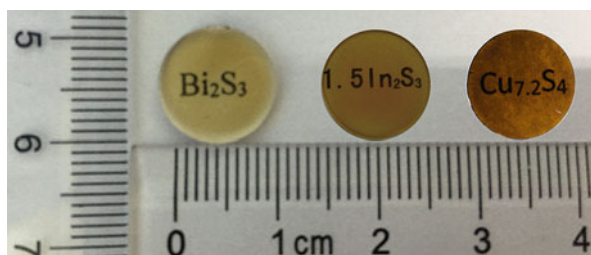


Fig. 31 Typical XRD pattern of the as-prepared glass doped CuGaS_2 quantum dots

Fig. 32 The images of the glasses doped Bi_2S_3 , In_2S_3 , and $\text{Cu}_{7.2}\text{S}_4$ quantum dots



(Bianchi et al. 1997). Boccaccini et al. (2005) for the first time reported borosilicate glass matrix composites containing a significant amount of multiwall carbon nanotubes by a sol-gel process. They also studied the densification behavior of carbon nanotubes/borosilicate glass mixtures.

Thomas et al. (2009) employed three different silicate precursors to produce dense borosilicate glass matrix composites containing up to 3 wt% of multiwalled carbon nanotubes by a sol-gel process. The dispersion of the carbon nanotubes aided an organic-inorganic binder; after densification, the borosilicate glass composites containing up to 2 wt% CNTs showed significant improvements in hardness and compression strength, as well as thermal conductivity, while percolation effects lead to a dramatic increase in electrical conductivity above 1 wt%.

Carbon dots (CDs) have received considerable attention (QDs) because of their unique properties such as high photo stability, low environmental toxicity, and excellent biocompatibility. Ma et al. (2015) prepared CDs doped sodium borosilicate

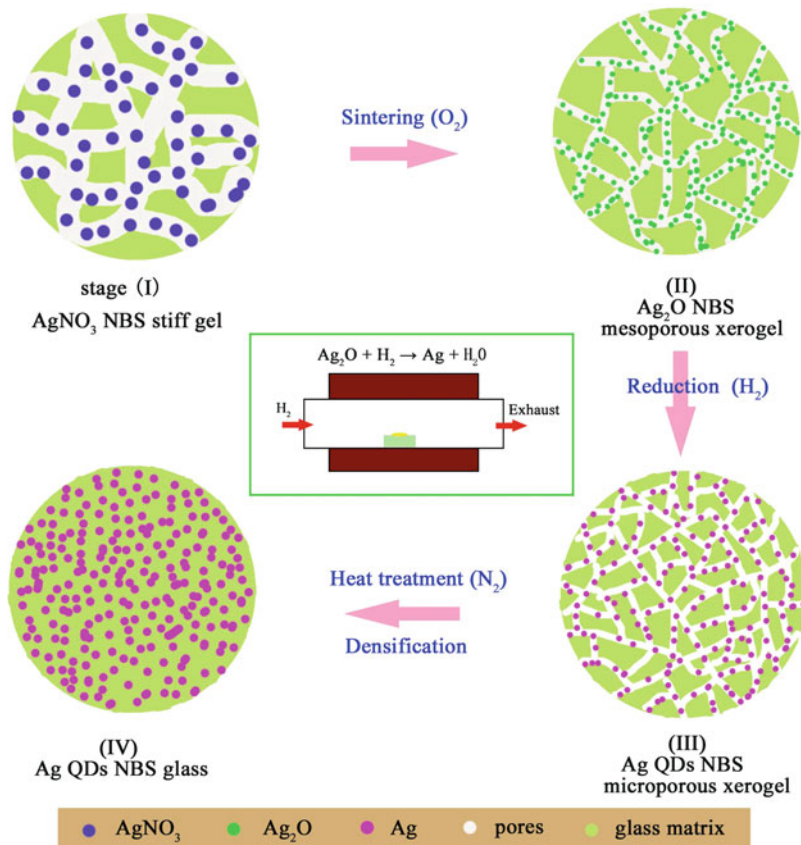


Fig. 33 A schematic illustration of the formation of the Ag QDs NBS glasses. The *inset* shows the apparatus for sintering Ag QDs NBS glasses

gel glasses by incorporating the CDs into sodium borosilicate networks. Images of the CD-NBS gel glasses captured through TEM and HRTEM demonstrated the uniformity and good dispersibility of the glasses, which exhibit similar statistical diameters of 2.9 ± 0.7 nm (Fig. 34).

Moreover, the PL properties of CD-NBS gel glasses, fluorescence wavelengths for all types of CD-NBS gel glasses, are independent of the excitation wavelength, whereas the PL intensity remarkably increased. Moreover, the fluorescence emission peak clearly redshifts from 550 nm to 600 nm for 5% and 70 wt% CD-NBS gel glasses, when the doping concentration of CDs increases (Fig. 35). Significantly, using surface analytical techniques, such as FT-IR and XPS spectroscopy, revealed that the PL properties of CD-NBS gel glasses are mainly influenced by the surface functional groups: surface modification can result in a redshift of CD emission in CD-NBS gel glasses (Fig. 36).

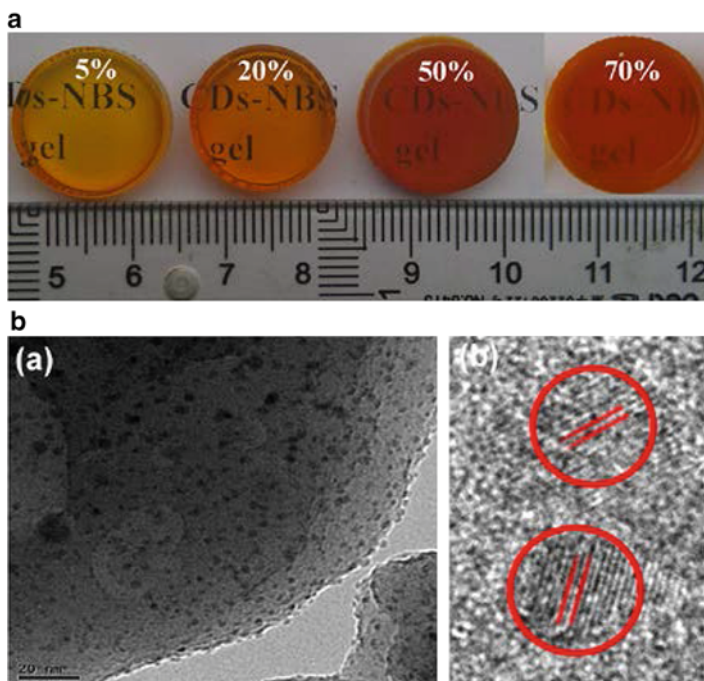


Fig. 34 (a) Optical photographs upon visible light of CD-NBS gels doped with various ratios of CDs (drying temperature 100 °C) (b) The TEM image and HRTEM image of prepared CD-NBS gel glass

In addition, the enhancement of the fluorescent QYs to 45%, 64% and 78% for 20 wt%, 50 wt% and 70 wt% CD-NBS gel glasses, respectively, from 25% for 5 wt% CD-NBS gel glasses were observed under excitation at 460 nm. Compared with the average lifetime and QYs of CDs, that of CD-NBS gel glasses with high dopant concentration of CDs are longer, so it can prevent solid-state luminescence quenching at some level.

More importantly, to use CD-NBS gel glasses with strong PL emission and high QY, we have developed CD-based W-LEDs (White Light-Emitting-Diode) by combining the yellow-emitting CD-NBS gel glasses with blue GaN-based LED chips (Fig. 37). For their practical application, the resulting W-LEDs exhibited the CIE (Commission Internationale de L'Eclairage) of (0.32, 0.33), which were close to that of balanced white-light emission (0.33, 0.33), with maximum LE exceeding 58.1 lmW^{-1} at the CCT of $\sim 6190 \text{ K}$ and with the CRI up to 78.9. These results would offer a new kind of CD-NBS gel glass that could become an alternative material for LEDs compared to the most commonly reported CD hybrid powder and films.

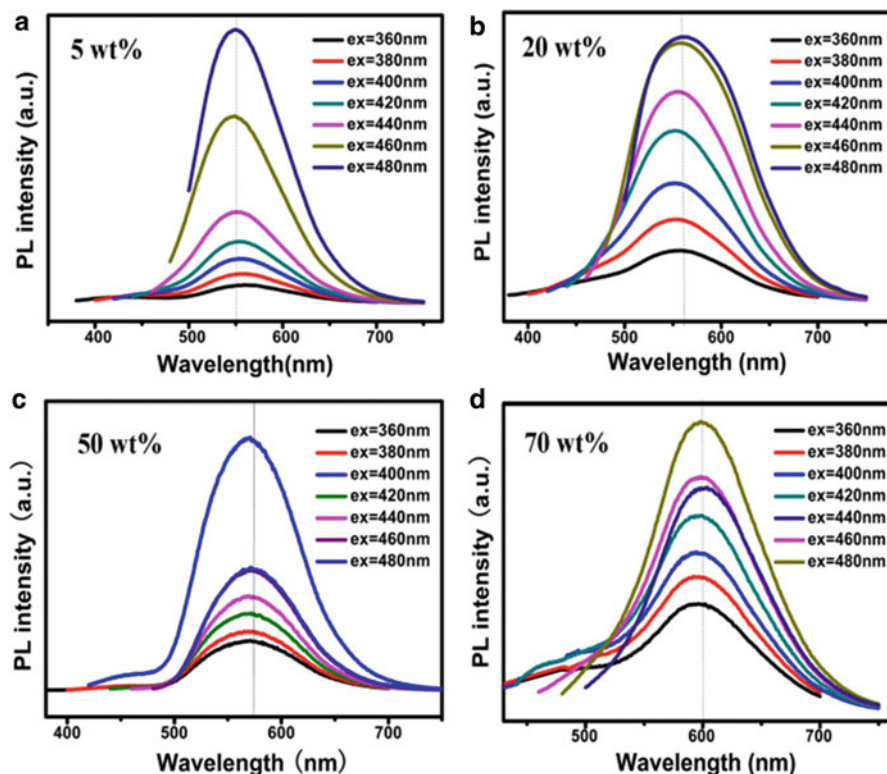


Fig. 35 PL emission spectra of the CD-NBS gel glasses with various CD loading fractions of (a) 5 wt%, (b) 20 wt%, (c) 50 wt%, and (d) 70 wt% under different excitation wavelengths recorded from 360 to 480 nm in 20 nm increments

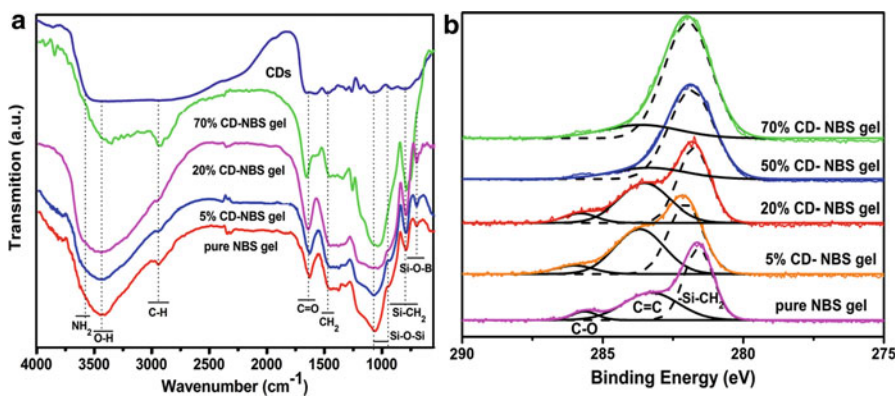


Fig. 36 (a) FTIR spectra (b) high-resolution XPS spectra of C 1s level for CD-NBS gel glass with different ratios of CDs

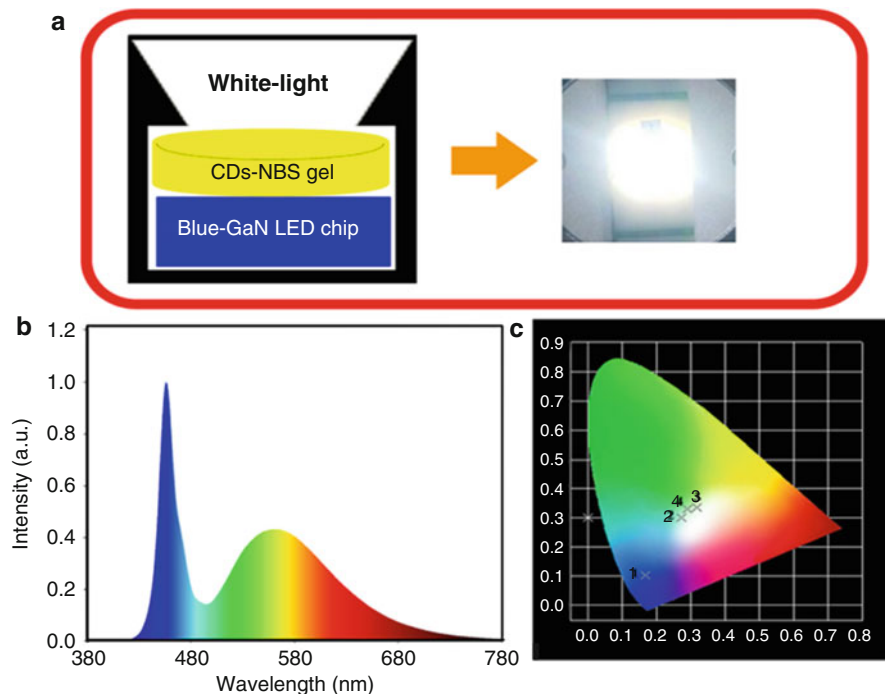


Fig. 37 (a) Fabrication strategy of W-LEDs based on CD-NBS gels with blue GaN LED chip and the photograph of a device. (b) Emission spectrum of the white LED lamp (color figure online) 50 wt% CD-NBS gels and (c) the CIE of CD-NBS gel glasses with different loading fraction of CDs on the CIE chromaticity chart: (1) 5%, (2) 20%, (3) 50%, (4) 70 wt%, respectively

Concluding Remarks

As described above, research works have demonstrated the feasibility and advantage of the sol-gel process combined with atmosphere control heat treatment to fabricate bulk and transparent borosilicate glass containing various kinds of nanoparticles in different valences, sizes, and multielements at relatively low heat-treatment temperatures. However, the important problem to shorten the whole experimental period remains to be solved.

References

- Angeli F, Villain O, Schuller S, Charpentier T, Ligny DD, Bresse L, Wondraczek L. Effect of temperature and thermal history on borosilicate glass structure. *Phys Rev B*. 2012;85:054110.
- Bartl MH, Gatterer K, Fritzer HP, Arafa S. Investigation of phase separation in Nd^{3+} doped ternary sodium borosilicate glasses by optical spectroscopy. *Spectrochim Acta, Part A*. 2001;57:1991–9.

- Brinker CJ, Scherer GW. Sol-gel science, 1990[J]. The physics and chemistry of sol-gel processing, 1990.
- Bianchi V, Goursat P, Sinkler W, Monthieux M, Ménessier E. Carbon-fibre-reinforced (YMAS) glass-ceramic matrix composites. I. Preparation, structure and fracture strength. *J Eur Ceram Soc.* 1997;17:1485–500.
- Boccaccini AR, Acevedo DR, Brusatin G, Colomboc P. Borosilicate glass matrix composites containing multi-wall carbon nanotubes. *J Eur Ceram Soc.* 2005;25:1515–23.
- Boccaccini AR, Thomas BJC, Brusatin G, Colombo P. Mechanical and electrical properties of hot-pressed borosilicate glass matrix composites containing multi-wall carbon nanotubes. *J Mater Sci.* 2007;42:2030–6.
- Bureau G, Delaye JM, Peugot S, Calas G. Molecular dynamics study of structural changes versus deposited energy dose in a sodium borosilicate glass. *Nucl Instrum Methods Phys Res Sect B.* 2008;266:2707–10.
- Cartaa D, Knowlesb JC, Smith ME, Newport RJ. Synthesis and structural characterization of P_2O_5 -CaO- Na_2O sol-gel materials. *J Non-Cryst Solids.* 2007;352:1141–9.
- Chen S, Akai T, Kadono K, Yazawa T. Reversible control of silver nanoparticle generation and dissolution in soda-lime silicate glass through X-ray irradiation and heat treatment. *Appl Phys Lett.* 2001;79:3687–9.
- Crivelli-Visconti I, Cooper GA. Mechanical properties of a new carbon fibre material. *Nature.* 1969;221:754–5.
- Doweidar H, Meikhaail MS, Holland D. Structural aspects of sodium borosilicate glasses. *J Non-Cryst Solids.* 1988;101:280–6.
- Efimov AM, Pogareva VG. Water-related IR absorption spectra for some phosphate and silicate glasses. *J Non-Cryst Solids.* 2000;275:189–98.
- Epifani M, Carlino E, Blasi C, Giannini C, Tapfer L, Vasanelli L. Sol-gel processing of Au nanoparticles in bulk 10 B_2O_3 -90 SiO_2 glass. *Chem Mater.* 2001;13:1533–9.
- Gaafar MS, Marzouk SY. Mechanical and structural studies on sodium borosilicate glasses doped with Er_2O_3 using ultrasonic velocity and FTIR spectroscopy. *Phys B.* 2007;388:294–302.
- Gao HH, Xiang WD, Ma X, Ma L, Huang YY, Ni HB, Shi XF, Chen GX, Liang XJ. Sol-gel synthesis and third-order optical nonlinearity of Au nanoparticles doped monolithic glass. *Gold Bull.* 2015;48:153–9.
- Grandjean A, Malki M, Montouillout V, Debruycker F, Massiot D. Electrical conductivity and ^{11}B NMR studies of sodium borosilicate glasses. *J Non-Cryst Solids.* 2008;354:1664–70.
- Hayashi A, Nakai M, Tatsumisago M, Minami T, Himei Y, Miura Y, Katada M. Structural investigation of SnO - B_2O_3 glasses by solid-state NMR and X-ray photoelectron spectroscopy. *J Non-Cryst Solids.* 2002;306:227–37.
- Hervig RL, Navrotsky A. Thermochemistry of sodium borosilicate glasses. *J Am Ceram Soc.* 1985;68:314–9.
- Heshmatpuor F, Adelkhani H, Jangholi M. Studying of optical and morphological properties of SiO_2 - MO_x (M: Co/Cu) glasses prepared by the sol-gel method. *J Non-Cryst Solids.* 2011;357:1409–13.
- Irwin AD, Holmgren JS, Zerda TW, Jonas J. Spectroscopic investigations of borosiloxane bond formation in the sol-gel process. *J Non-Cryst Solids.* 1987;89:191–205.
- Irwin AD, Holmgren JS, Jonas J. Solid state ^{29}Si and ^{11}B NMR studies of sol-gel derived borosilicates. *J Non-Cryst Solids.* 1988;101:249–54.
- Klein LC. Sol-gel optics: processing and applications. Berlin: Springer; 1994.
- Korgel BA. Materials science: composite for smarter windows. *Nature.* 2013;500:278–9.
- Liu SM, Zhao GL, Ying H, Wang JX, Han GR. Effects of mixed alkaline earth oxides additive on crystallization and structural changes in borosilicate glasses. *J Non-Cryst Solids.* 2008;354:956–61.
- Lordés A, García G, Gazquez J, Milliron DJ. Tunable near-infrared and visible-light transmittance in nanocrystal-in-glass composites. *Nature.* 2013;500:323–6.

- Ma L, Xiang WD, Gao HH, Pei L, Ma X, Huang YY, Liang XJ. Carbon dot doped sodium borosilicate gel glasses with emission tunability and their application in white light emitting diodes. *J Mater Chem C*. 2015;3:6764–70.
- Mangin S, Gottwald M, Lambert CH, Steil D, Uhlir V, Pang L, Hehn M, Alebrand S, Cinchetti M, Malinowski G, Fainman Y, Aeschlimann M, Fullerton EE. Engineered materials for all-optical helicity-dependent magnetic switching. *Nat Mater*. 2014;13:286–92.
- Marzouk SY, Seoudi R, Said DA, Mabrouk MS. Linear and nonlinear optics and FTIR characteristics of borosilicate glasses doped with gadolinium ions. *J Opt Mater*. 2013;35:2077–84.
- Matsuoka J, Toyoda M, Yoshida S. Composition dependence of the optical absorption spectra of cupric ion in sodium borosilicate glass melts. *J Non-Cryst Solids*. 2008;354:255–8.
- Milberger ME, Keefe JGO, Verhelst RA, Hooper HO. Boron coordination in sodium borosilicate glasses. *Phys Chem Glasses*. 1972;13:79–84.
- Mishra RK, Sudarsan V, Kaushik CP, Tyagi AK, Tomar BS, Das D, Raj K. Ionic transport behavior of BaO containing sodium borosilicate glasses. *J Non-Cryst Solids*. 2007;353:1450–3.
- Miura Y, Kusano H, Nanba T, Matsumoto S. X-ray photoelectron spectroscopy of sodium borosilicate glasses. *J Non-Cryst Solids*. 2001;290:1–14.
- Muralidharan P, Venkateswarlu M, Satyanarayana N. AC conductivity studies of lithium borosilicate glasses: synthesized by sol–gel process with various concentrations of nitric acid as a catalyst. *Mater Chem Phys*. 2004;88:138–44.
- Nesbitt HW, Bancroft GM, Henderson GS, Ho R, Dalby KN, Huang Y, Yan Z. Bridging, non-bridging and free (O_2^-) oxygen in Na_2O-SiO_2 glasses: an X-ray Photoelectron Spectroscopic (XPS) and Nuclear Magnetic Resonance (NMR) study. *J Non-Cryst Solids*. 2011;357:170–80.
- Osaka A, Yuasa M, Miura Y, Takahashi K. Sodium borosilicate glasses prepared by the sol–gel process. *J Non-Cryst Solids*. 1988;100:409–19.
- Park JH, Lee SJ. Mechanism of preventing crystallization in low-firing glass/ceramic composite substrates. *J Am Ceram Soc*. 1995;78:1128–30.
- Pei L, Xiang WD, Zhao XL, Liang XJ, Yang XY, Liu HT, Chen ZP, Xie CP, Ma X, Zhang CL, Ma L, Zhao JL. Sol–gel synthesis of silver nanocrystals embedded in sodium borosilicate monolithic transparent glass with giant third-order optical nonlinearities. *Mater Res Bull*. 2014;59:154–61.
- Prasad PN. Quantum-confined materials. In: Prasad PN, editor. *Nanophotonics*. Hoboken: Wiley; 2004. p. 79–127.
- Rajesh D, Ratnakaram YC, Balakrishna A. Er^{3+} -doped strontium lithium bismuth borate glasses for broadband 1.5 μm emission—structural and optical properties. *J Alloys Compd*. 2013;56:22–7.
- Rao TGVM, Kumar AR, Neeraja K, Veeraiha N, Reddy MR. Optical and structural investigation of Eu^{3+} ions in Nd^{3+} co-doped magnesium lead borosilicate glasses. *J Alloys Compd*. 2013;557:209–17.
- Rumori P, Deroide B, Abidi N, El Mkami H, Zanchetta JV. Mn^{2+} electron paramagnetic resonance study of a sodium borosilicate glass prepared by the sol–gel method. *J Phys Chem Solids*. 1998;59:959–67.
- Saad EA, El Batal FH, Fayad AM, Moustafa FA. Infrared absorption spectra of some Na-borosilicate glasses containing AgBr and Cu_2O (photochromic glasses) in addition to one of transition metal oxide. *J Silicon*. 2011;3:85–95.
- Sakka S. *Handbook of sol–gel science and technology: processing, characterization and applications*. Kluwer Academic Publishers; 2005.
- Selvan ST, Hayakawa T, Nogami M, Kobayashi Y, Liz-Marzán LM, Hamanaka Y, Nakamura A. Sol–gel derived gold nanoclusters in silica glass possessing large optical nonlinearities. *J Phys Chem B*. 2002;106:10157–62.
- Song CF, Lu MK, Yang P, Xu D, Yuan DR, Zhou GJ, Gu F. Green emission from Cr, Dy co-doped sol–gel SiO_2 glasses. *J Mater Sci Eng B-ADV*. 2003;97:64–7.
- Soraru GD, Dallabona N, Gervais C, Babonneau F. Organically modified $SiO_2-B_2O_3$ gels displaying a high content of borosiloxane (BO-Si) bonds. *Chem Mater*. 1999;1:910–9.

- Soraru GD, Babonneau F, Gervais C, Dallabona N. Hybrid $\text{RSiO}_{1.5}/\text{B}_2\text{O}_3$ gels from modified silicon alkoxides and boric acid. *J Sol-Gel Sci Technol.* 2000;18:11–9.
- Speranza G, Minati L, Chiasera A, Ferrari MG, Righini C, Ischia G. Quantum confinement and matrix effects in silver-exchanged soda lime glasses. *J Phys Chem C.* 2009;113:4445–50.
- Sun K, Wang LM, Eming RC, Weber WJ. Electron irradiation induced phase separation in a sodium borosilicate glass. *Nucl Instrum Methods Phys Res Sect B.* 2004;218:368–74.
- Thomas BJC, Shaffer MSP, Boccaccini AR. Sol-gel route to carbon nanotube borosilicate glass composites. *Compos Part A Appl Sci Manufac.* 2009;40:837–45.
- Villegas MA, Fernandez Navarro JM. Characterization and study of $\text{Na}_2\text{O}-\text{B}_2\text{O}_3-\text{SiO}_2$ glasses prepared by the sol-gel method. *J Mater Sci.* 1988;23:2142–52.
- Wu XW, Youngman RE, Dieckmann R. Sodium tracer diffusion and ^{11}B NMR study of glasses of the type $(\text{Na}_2\text{O})_{0.17}(\text{B}_2\text{O}_3)_x(\text{SiO}_2)_{0.83-x}$. *J Non-Cryst Solids.* 2013;378:168–76.
- Xiang WD, Zhao HJ, Zhong JS, Yang XY, Guo YQ, Luo HY, Liang XJ. The preparation and the third-order optical nonlinearities of the sodium borosilicate glass doped with CuInS_2 quantum dots. *J Am Ceram Soc.* 2012;95:1588–94.
- Xiang WD, Zhao HJ, Zhong JS, Luo HY, Zhao XL, Chen ZP, Liang XJ, Yang XY. Synthesis and third-order optical nonlinearities of In_2S_3 quantum dots. *J Alloys Comp.* 2013;553:135–41.
- Xiang WD, Gao HH, Ma L, Ma X, Huang YY, Pei L, Liang XJ. Valence state control and third-order nonlinear optical properties of copper embedded in sodium borosilicate glass. *ACS Appl Mater Inter.* 2015;7:10162–8.
- Yang XY, Xiang WD, Zhang XY, Liang XJ, Liu HT, Dai SX, Chen FF. Third-order optical nonlinearity of CdS nanocrystals embedded in sodium borosilicate glass studied by the Z-scan technique. *J Mater Res.* 2010;25:491–9.
- Yang XY, Xiang WD, Zhao HJ, Zhang XY, Liang XJ, Dai SX, Chen FF. Third-order nonlinear optical properties of Bi_2S_3 nanocrystals doped in sodium borosilicate glass studied with Z-scan technique. *Mater Res Bull.* 2011a;46:355–60.
- Yang XY, Xiang WD, Zhao HJ, Liu HT, Zhang XY, Liang XJ. Nonlinear saturable absorption of the sodium borosilicate glass containing Bi_2S_3 nanocrystals using Z-scan technique. *J Alloy Compd.* 2011b;509(26):7283–9.
- Yang XY, Xiang WD, Liu HT, Zhao HJ, Zhang XY, Liang XJ. Microstructures and the third-order optical nonlinearities of semimetal Bi nanocrystals in the sodium borosilicate glass. *Mater Lett.* 2011c;65(12):1959–62.
- Yang XY, Liu HT, Zhao HJ, Zhang XY, Liang XJ, Xiang WD. Fabrication and third-order optical nonlinearities of $\text{Na}_2\text{O}-\text{B}_2\text{O}_3-\text{SiO}_2$ glasses containing metallic Bi, Bi_2O_3 and Bi_2S_3 crystals. *Mater Chem Phys.* 2011d;129:121–9.
- Yin DW, Pei L, Liu Z, Yang XY. Glass hybrid nanocomposites containing metallic Ag-Ga nanocrystals: synthesis, microstructure, and photoluminescence. *J Am Ceram Soc.* 2014;97:3489–93.
- Yun YH, Bray PJ. Nuclear magnetic resonance studies of the glasses in the system $\text{Na}_2\text{O}-\text{B}_2\text{O}_3-\text{SiO}_2$. *J Non-Cryst Solids.* 1978;27:363–80.
- Yusufali C, Kshirsagar RJ, Jagannath MRK, Dutta RS, Dey GK. Infrared and X-ray photoelectron spectroscopy studies on sodium borosilicate glass interacted with thermally oxidized aluminides formed on Alloy 690. *J Non-Cryst Solids.* 2013;366:54–8.
- Zeng H, Qiu J, Ye Z, Zhu C, Gan F. Irradiation assisted fabrication of gold nanoparticles-doped glass. *J Cryst Growth.* 2004;267:156–60.
- Zhang CL, Xiang WD, Luo HY, Liu HT, Liang XJ, Ma X, Chen ZP, Li JS, Gao HH, Ma L. Third-order optical nonlinearity of $\text{Na}_2\text{O}-\text{B}_2\text{O}_3-\text{SiO}_2$ glass doped with lead nanoparticles prepared by sol-gel method. *J Alloys Compd.* 2014;602:221–7.
- Zhao CH, Zhang BP, Wang SJ, Shang PP, Li S, Yan LP. Microstructure and optical absorption property of the Cu/SiO_2 nano-films. *Mater Des.* 2011;32(2):947–50.
- Zhao HJ, Xiang WD, Zhong JS, Yang X, Guo YQ, Liang XJ, Huang HY, Luo HY, Zhao XL, Chen ZP. Preparation and the third-order optical nonlinearities of the sodium borosilicate glass doped with $\text{Cu}_{7.2}\text{S}_4$ quantum dots. *J Non-Cryst Solids.* 2012;358:2641–9.

- Zhong JS, Xiang WD, Zhao HJ, Liang XJ, Zhao WG, Chen GX. Preparation and nonlinear optical properties of indium nanocrystals in sodium borosilicate glass by the sol-gel route. *Mater Res Bull.* 2012a;47:3691-6.
- Zhong JS, Xiang WD, Zhao HJ, Zhao WG, Chen GX, Liang XJ. Synthesis, characterization, and nonlinear optical properties of copper quantum dots embedded in sodium borosilicate glass. *J Alloy Compd.* 2012b;537:269-74.
- Zhong JS, Xiang WD, Chen ZQ, Zhao HJ, Liang XJ. Structural, linear and third-order nonlinear optical properties of Cu nanocrystal in sodium borosilicate glass. *Mater Sci Eng B.* 2013a;178:998-1003.
- Zhong JS, Xiang WD, Chen ZP, Xie CP, Luo L, Liang XJ. Microstructures and third-order optical nonlinearities of Cu₂In nanoparticles in glass matrix. *J Alloy Compd.* 2013b;572:137-44.
- Zhong JS, Xiang WD, Liang XJ, Chen ZP, Zhao WG. Na₂O-B₂O₃-SiO₂ glass doped with In and Cu₂In nanoparticles prepared by sol-gel method. *J Non-Cryst Solids.* 2013c;361:124-9.
- Zhong JS, Ma X, Lu HW, Wang X, Zhang SL, Xiang WD. Preparation and optical properties of sodium borosilicate glasses containing Sb nanoparticles. *J Alloy Compd.* 2014a;607:177-82.
- Zhong JS, Zhao HJ, Zhang CL, Ma X, Pei L, Liang XJ, Xiang WD. Sol-gel synthesis and optical properties of CuGaS₂ quantum dots embedded in sodium borosilicate glass. *J Alloy Compd.* 2014b;610:392-8.